João Manuel Martins Neto

Licenciado em Engenharia de Micro e Nanotecnologias

Large-Area Alignment of Nanowires for High-Performance Flexible Electronics

Dissertação para obtenção do Grau de Mestre em
Engenharia de Micro e Nanotecnologias

Orientador: Prof. Ravinder Dahiya, Professor, University of Glasgow

Co-orientadores: Prof. Pedro Barquinha, Associate Professor, FCT-UNL

FACULDADE DE CIÊNCIAS E TECNOLOGIA
UNIVERSIDADE NOVA DE LISBOA

October 2019

Large-Area Alignment of Nanowires for High-Performance Flexible Electronics

Acknowledgments

Firstly, i would like to thank the BEST group leader, Prof. Ravinder Dahiya, for receiving me in his great multidisciplinary group, which made this work possible and for the opportunity to keep working with this amazing team. A special thanks to William that showed me what it is to be a researcher and that good research takes time, good luck with your group and never lose the inspirational side that you have. Not less important, Dr. Dhayalan for the support and help in all the matters during the last months and Ayoub for the long hours of clean room that we shared.

Agradeço ao Dr. Pedro Barquinha pela oportunidade que me deu no estágio de 3º ano, foi uma das chaves que incentivou o trabalho desenvolvido nesta tese e pelas sugestões fornecidas neste trabalho.

A toda a minha família que sempre me ajudou em qualquer momento de necessidade, principalmente os meus pais que prometeram dar-me tudo o que tinham ao seu alcance para eu ter sucesso, completo assim a promessa que vos fiz de terminar o curso em 5 anos com toda a responsabilidade que isso traria. Descansem que voltarei sempre a casa!

Ao meu irmão, que sempre vi como um exemplo, parabéns e obrigado pelas fantásticas pestes que trouxeste ao mundo, irei tratar deles como se fossem meus.

Aos meus tios por todas as descargas que me deixaram no Serrado e por essa piscina no monte!

Por fim, à pessoa de quem tenho vindo seguindo as pisadas, a minha Madrinha Sónia, um obrigado que vem desde o momento que estive contigo a ler a lista dos cursos até ao dia em que submeti esta tese e completei o curso que escolhi a teu lado 5 anos antes…

A todo o pessoal que a universidade e o Serrado me trouxeram, fica um desejo de boa sorte e agradecimento por todos os momentos que passamos na Gloriosa FCT, só nós saberemos todas as risadas e lágrimas que soltamos estes anos.

Ao Sérgio, por teres sido mais que um padrinho, foste um amigo e irmão, por todos os conselhos, momentos, ensinamentos, jantares, noites…Obrigado por teres tido a influência que tiveste na minha vida e de teres criado com a Sofia aquilo que foi a nossa família. À Barbaracita e ao Alejandro digo-vos que foi uma honra ter partilhado tantas horas de estudo, praxes, jantares e momentos que só mesmo irmãos passariam, boa sorte nos vossos caminhos e que nos encontremos todos num futuro muito próximo. À Carolina e Diogo fica o agradecimento de quem sempre se preocupou com vocês e lembrem-se de que têm o mundo aos vossos pés, basta quererem, orgulho em vocês putos.

Ao Zé, colega de turma do secundário e de casa desde o início destes anos, muita sorte neste novo caminho e que trates bem dos teus colegas de casa, carrega grutas.

A todos aqueles que trabalharam comigo, especialmente na CoPe, nunca esqueçamos todos os momentos que tivemos de ultrapassar e os feitos atingidos nesse ano épico. Ao Matinhus Matex, lacaio, obrigado por teres sido dos poucos a acompanhar-me até ao fim no Serrado e pela companhia nas equipas que partilhamos.

A todo o pessoal de Beja que não tiveram presentes na universidade mas continuaram sempre presentes dentro de mim, orgulho no nosso grupo que se mantêm unido a mais de uma década…

Para terminar, agradecer a todo o pessoal restante de nano que não consegui agradecer e ao pessoal de materiais principalmente a Lena Lena, o Fred Fox e o Moura. Não esquecendo o puto Adriano por todas essas camadas que apanhamos juntos. Teria de ser mais que uma página para agradecer a todos aqueles que fizeram parte do que foi os melhores anos da minha vida e o orgulho que levo, num ambiente que só mesmo a FCT é que podia oferecer.

"Sê todo em cada coisa. Põe quanto és
No mínimo que fazes."

Ricardo Reis, in "Odes"

Abstract

Inorganic semiconducting nanowires are suitable components for high-performance flexible electronics, due to their attractive and tuneable physical, chemical and electrical properties. The key requirement to attain such applications is the controlled transfer of NWs over flexible materials, which needs to ensure three critical aspects, (1) controlled location, (2) alignment and (3) density. Several techniques exist to align high-aspect ratio 1D nanostructures in a scalable, easy, fast and low-cost way, such as dielectrophoresis (DEP) that consists in an electric field induced alignment.

During the current work at the University of Glasgow, a modified DEP technique was used to align V_2O_5 nanowires. The aim was to use a dip coating modified DEP large-scale assembly over flexible substrates. By assembling the nanowires with microelectrodes positioned through a dielectric layer, the templated nanowires could be used for fabrication of devices without interference of alignment electrodes and fabricated structures. The setup consists of electrodes over polyimide sheet with 4 arrays of different gaps. The fabricated substrate is fixed in a carrier which is dip-coated through a vertical movement in a V_2O_5 NW/DI water solution. An AC signal of 300 V, 1 MHz and a withdrawal speed of 100 µm/s are the optimized DEP parameters. SEM images revealed a nanowire density of 15 NW/µm with 96% alignment.

Given the thermal sensitivity of V_2O_5, structures with aligned NWs were used as a temperature sensor with a resulting temperature coefficient of resistance of -0.97 and -0.1 % K^{-1} for contact and contactless setup, respectively.

Keywords: Nanowires alignment, dielectrophoresis, large-area transfer, temperature sensor.

Resumo

Nanofios (NF) semicondutores inorgânicos são componentes adequados para eletrónica flexível de alto desempenho, devido às suas propriedades físicas, químicas e elétricas atraentes e ajustáveis. O principal requisito para atingir tais aplicações é a transferência controlada de nanofios sobre materiais flexíveis, que precisa garantir três aspectos críticos: (1) localização controlada, (2) alinhamento e (3) densidade. Existem várias técnicas para alinhar nanoestruturas 1D, de maneira escalável, fácil, rápida e de baixo custo, como a dieletroforese (DEP) que consiste num alinhamento induzido por campo elétrico.

Durante o trabalho atual na Universidade de Glasgow, uma técnica de DEP modificada foi usada para alinhar nanofios de V_2O_5. O objetivo era usar a técnica modificada de DEP em grande escala por revestimento por imersão sobre substratos flexíveis. Ao depositar os nanofios com microelétrodos posicionados através de uma camada dielétrica, estes podem ser usados para a fabricação de dispositivos sem interferência entre elétrodos de alinhamento e estruturas fabricadas por cima dos nanofios. A configuração consiste em elétrodos fabricados num substrato de poliimida com 4 matrizes de diferentes espaçamento entre elétrodos. O substrato fabricado é fixado num transportador que é imerso através de um movimento vertical numa solução de água desionizada com nanofios de V_2O_5. Um sinal AC de 300 V, 1 MHz e a velocidade do transportador de 100 μm/s são os parâmetros DEP otimizados. As imagens SEM revelaram uma densidade de 15 NF/μm com alinhamento de 96%.

Dada a sensibilidade térmica do V_2O_5, estruturas com NF alinhados foram usadas como sensor de temperatura com um coeficiente de temperatura de resistência de -0,97 e -0,1 % K^{-1} com configuração por contato e sem contato, respectivamente.

Palavras-Chave: Alinhamento de nanofios, dieletroforese, transferência de larga escala, sensor de temperatura.

Contents

List of Figures

List Of Tables

Abbreviations and Symbols

1D - One dimension
3D – Three dimensions
AC – Alternating current
DC – Direct current
DEP - Dielectrophoresis
DI – Deionized
E – Electric Field
EDS – X-ray spectroscopy
F_{CM} – Clausius-Mossotti factor
IR – Infrared
NW - Nanowire
NW-FET – Nanowire-Field effect transistor
p – dipole moment
PET – Polyethylene terephthalate
PI – Polyimide
Rpm – rotations per minute
SEM – scanning electron microscopy
TCR – Temperature coefficient of resistance
UV – Ultraviolet
ν– Particle volume
Via – Vertical interconnect access
V_{pp} – Voltage peak-to-peak
α – polarizability
ε_m – Permittivity of medium
ε_p - Permittivity of particle
σ_m – Conductivity of medium
σ_p – Conductivity of particle
ω – Angular frequency

Motivation and Objectives

The effort made by researchers in developing nanomaterials and improving their manipulation techniques had made flexible electronics industry a reality. This is an emerging market with almost $31.7 billion profit in 2018 and it's expected to reach $77.3 billion by 2029 according to IDTechEx.

The integration of nanomaterials as basic building blocks for devices of flexible electronics is of most importance, as they enable the fabrication of the most used active components like transistors and diodes. Organic materials are on the base of flexible electronics and are used as substrates or active-materials like n-type semiconductor. However, for high-performance applications like displays or electronic skin they are not suitable, as they have low carrier mobilities, when compared to inorganic semiconducting materials. By employing inorganic nanomaterials in a controllable way and printing interconnections, high–performance flexible components like transistors can be created and connected to other components to create a complex system.

Nanowires are high aspect-ratio nanostructures, with tuneable electrical and geometrical properties, they can have cost-effective synthesis and are suitable for flexible devices. Nevertheless, manipulation of such structures with precision and patterned assembly on flexible substrates in a large-scale apparatus, is still a challenge.

Therefore, the objective of this work is the alignment of nanowires, using an electric field, with a known technique called dielectrophoresis.

The main goals of this work are bulleted below:

- Patterned alignment of high aspect-ratio nanostructures e. g. nanowires through a dielectric layer with dielectrophoresis (DEP) technique.
- Automated dip-coating DEP process for patterned alignment on flexible substrates with reusable electrodes for roll-to-roll application.
- Fabrication of vanadium pentoxide (V_2O_5) nanowires array as basic building block for temperature sensors (Bridging two pads).
- Passive-matrix addressing of 900 V_2O_5 NW pixels through Via-bridges.

1. Introduction

1.1. Large-scale flexible electronics

Flexible electronics are characterized by being thin, light-weight and having high bendability or even stretchability while their performance remains constant.

The development on the synthesis of novel nanomaterials led to a revolution on this area, application of such materials on flexible substrates results in a wide variety of complex systems like electronic skin [1], sensors [2,3] or photovoltaics [4].

The substrates used can go to 20 μm thickness or less and can be polymers like PET (Polyethylene terephthalate), PI (Polyimide) or paper. Such devices are very thin and different features can be added depending on the materials used, for example, transparent polymers allow fabrication of transparent devices.

Fabrication techniques are also important, printing conductive inks on flexible substrates with roll-to-roll technique will enable low-cost, fast and large-scale manufacturing [5] by replacing expensive clean room techniques. This will allow flexible electronics to be fabricated as easy as printing a newspaper. There are however some challenges to overcome. Problems like ink formulation with different nanomaterials, sintering of such inks on low-thermal resistance polymers, manipulation of nanostructures for basic building blocks or adhesion and encapsulation of such structures are problems that remain to be solved. [6]

1.1.1. Nanowire based flexible electronics

1D nanostructures are characterized by having 2 dimensions in the nanometer scale (<100 nm) and a third with dimensions that can be more than 1000 times higher. Structures like nanowires (NWs), nanotubes and nanoribbons are inserted in this group. Materials in such structures have different electrical, optical, mechanical and other functional properties comparing to their bulk (3D) compositions.

The high surface to volume ratio of nanowires makes these structures highly sensitive to external effects making them very promising in sensors, detectors, photovoltaics and catalysts.

Due to the small dimensions of nanowires they will experience a quantum confinement effect. The nanowire dimensions will reach values close to the electron mean free path, leading to a change in the electron transport mechanism across the nanowires. This is highly dependent on the length and diameter of the nanowire, as diameters can reach just a few nanometres . [8-10]

Nanowires can be integrated on many applications due to their combined electrical and mechanical properties, a wide number of publications with nanowires of different materials has been published, a neural silicon NW-FET was developed by Navaraj et al [10], transparent NW electrodes [11] and many others reviewed on [12].

1.2. Alignment techniques of 1D nanostructures

High-performance devices and applications require oriented conformations of 1D nanostructures. Integration of these structures with controllable and patterned disposition is crucial to fabrication of devices on different types of substrates.

There are several advantages in aligning nanostructures. In a random network there is a high probability of electrons to go around the NW network decreasing its performance. [13] It's preferable that the conduction occurs on the least number of entities possible, a single nanowire can transport electrons faster than several nanowires connected between them. This is due to the junction resistance between

nanowires, which will increase the sheet resistance. The contact resistance can be lowered with thermal annealing that will increase the area of contact by fusing the nanowires together. The distribution thickness and density of these structures is important not only to create high-performance devices, but also to fabricate large-scale circuits with similar component performance. Also, optoelectronics applications require a control on the density and uniformity of the network, higher density means lower transmittance which can affect the optical properties of the device. Overlapping nanowires on the network can cause short-circuits and leakages in multi-layered device. [14-16]

In order to prevent this random distribution several techniques have been explored, like Langmuir-Blodgett (LB), contact printing, capillary printing, magnetic, electric-field induced and others reviewed on [13]. Most of these techniques can assemble the nanowires in a parallel way but they lack controllable and oriented positioning. Magnetic and electric field induced orientation can prevent this issue, but magnetic orientation requires that the particle is magnetized, thus, is not viable for the most electronic applications. A low cost, fast, simple and high-throughput method is required for a feasible industrial application.

The majority of nanomaterials used for flexible electronics are conducting or have polarizability characteristics, therefore an electric field induced alignment is highly favourable. Dielectrophoresis (DEP) can be used at room temperature with a variety of nanomaterials in a liquid dispersion, it's a low-cost method to align and pattern nanowires, can be scalable and doesn't affect the structure integrity.

1.2.1. Dielectrophoresis

The concept of dielectrophoresis was introduced by Herbert Pohl in 1951 and is the combination of the word "dielectric", with the Greek word "phoresis" that stands for force [16]. The main difference between DEP and standard electrophoresis is its application to neutral particles under an un-homogenous electric field. [17] Nevertheless, to guarantee an efficient use of this technology, the electromechanics between the materials used in such apparatus, when subject to an electric field must be fully understood.

When a perfect dielectric spheroid is subjected to an electric field, the opposite charges of the particle will be distributed in opposite directions with a distance d (depending on the magnitude of the electric field) creating a dipole that polarizes the particle. If this sphere is submersed in a fluidic dielectric material (e.g. DI water) with different dielectric constants and conductivities, a dipole moment (p) will be induced (Eq. 1) dependent on the volume of the particle (*v)*, the electric field (E) and polarizability (α).

The direction of the dipole moment is dependent on the dielectric properties of the materials involved in the process, Fig.1 represents the behaviour of the electric field lines when interacting with a cell. If the cell is less conductive than the field the current flux lines will tend to concentrate on the fluid avoiding the cell (Fig.1a) and the vector for the dipole moment will be opposite to the electric field. The contrary occurs when the lines go through the cell, which is more conductive than the surrounding medium (Fig.1b), this is valid for other types of particles and structures. The magnitude of this dipole moment depends on the polarizability of the particle defined by Eq. 2. Where ε_m is the medium permittivity and F_{CM} the Clausius-Mossotti factor.

$$p = \alpha v E \tag{1}$$

$$\alpha = 3\,\varepsilon_m \varepsilon_0\, F_{CM} \tag{2}$$

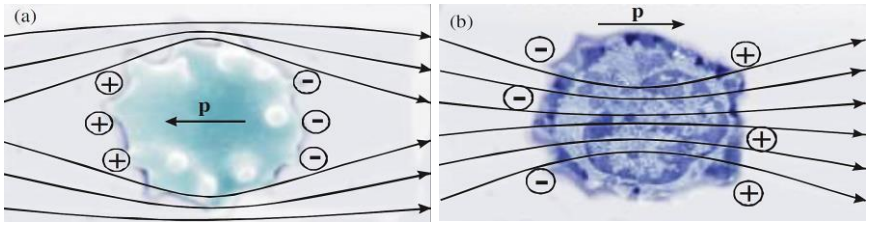

Figure 1 – a) Field lines avoiding the cell when the fluid is more conductive. **b)** Field lines penetrating the cell when the fluid is less conductive. [14]

The Clausius-Mossotti factor (F_{cm}) (Eq.3) defines the polarizability of the particle in relation to the medium, it is dependent on the permittivity of the medium and particle ($\varepsilon_{m,p}$). When F_{CM} is positive the particle is more polarizable than the fluid ($\varepsilon_p > \varepsilon_m$) and it will be attracted towards the high-density field, the opposite happens when $\varepsilon_p < \varepsilon_m$, in this case the particle will be repelled from these zones. [19-22] Equation 3 is for an ideal dielectric medium where there is no ohmic conduction of mobile charges, if energy losses are considered F_{CM} will be dependent on the complex permittivity's defined in equation 4, where $\sigma_{m,p}$ is the conductivity of the medium or particle, j is $\sqrt{-1}$ and ω the angular frequency of the signal.

$$F_{CM} = \frac{\varepsilon_P - \varepsilon_m}{\varepsilon_P + 2\varepsilon_m} \tag{3}$$

$$\varepsilon_P^* = \varepsilon_p - j\frac{\sigma_p}{\omega} \quad \& \quad \varepsilon_m^* = \varepsilon_m - j\frac{\sigma_m}{\omega} \tag{4}$$

The dependency on the frequency can be explained considering the same spheroid subject to a high frequency signal (>10 kHz). When the dipole is created the charges move in opposite directions, this movement requires time for the masses to move. A sinusoidal AC signal will change its polarization each half period. If the frequency is very high the charges will not have enough time to move and create the dipole as the charges cannot follow the electric field polarization. [19]

The spatial distribution of the electric field is another important factor since the opposite charges of the dipole are distanced and may experience different magnitude forces. Under an electric field the particle will experience a torque that will align the dipole parallelly to the field lines, however, this torque only occurs until the dipole aligns with the field lines. In a non-uniform electric field, the dipole charges will experience not only the torque but also a translational force, as the forces applied on both charges will be different. This is called *dielectrophoretic force* and defined by the Eq. 5, which depends on the volume of the particle (v), the real part of F_{CM} (Re (F_{CM})) and the square gradient of the electric field ($\nabla|E^2|$).

$$F_{DEP} = v\varepsilon_m Re\,(F_{CM})\nabla|E^2| \tag{5}$$

A brief explanation of the forces was made considering a sphere, however, in this work its pertinent to explore a model for 1D nanostructures. A nanowire will have similar behaviour as the sphere when exposed to the electric field, a dipole is induced when the surface charges move to its extremities, however, to quantify the DEP forces a different model must be assumed, a prolate spheroid is a reasonable approximation to a cylindrical particle with high aspect-ratio. Because the nanowire has a very high aspect ratio, the forces on the structure will be highly anisotropic and Re (F_{CM}) must be separated in two components, $F_{CM\text{-}Long}$ (Eq. 6) and $F_{CM-Short}$(Eq.7) which represents the long (length) and short-axis (radius) of the nanowire, respectively.

Depending on the relative position of the nanowire according to the gradient different magnitude of DEP forces are present. If the nanowire is parallel to the field gradient, the DEP force (translational) has a single component along the length of the nanowire and it will follow the direction of the field lines. When it is perpendicular to the field gradient the DEP force is based on the short-axis F_{CM}, the nanowire experiences a force perpendicular to its length-axis with the direction of the gradient. When the nanowire is not perpendicular or parallel both forces are involved in the process. The volume of nanowires is defined by Eq. 8 [21-23]

$$F_{CM-Long} = \frac{\varepsilon_P^* - \varepsilon_m^*}{\varepsilon_m^*} \tag{6}$$

$$F_{CM-Short} = 2\,\frac{\varepsilon_P^* - \varepsilon_m^*}{\varepsilon_P^* + 2\varepsilon_m^*} \tag{7}$$

$$v = \frac{1}{2} r_{NW}^2 L_{NW} \tag{8}$$

There are other forces beside the F_{DEP} that may negatively influence the alignment process. As particles get smaller Brownian motion which is originated by thermal energy has more impact on the particle. By inducing an electric field two forces occur, *Electrothermal flow* occurs when a high electric field is applied on the electrodes, which will dissipate power creating a localized heating, thus, increasing the temperature (electric currents will also create joule heating). This increase leads to a localized change of fluid parameters such as, density, viscosity, permittivity and conductivity leading to the creation of buoyancy, Coulomb and dielectric forces. *Electro-osmosis flow* occurs with the medium-electrode interaction, the voltage will attract electrolytes which settle on the surface of the electrode creating an electrical double layer. The electrolytes experience a force tangential to the electrode surface creating a movement which leads to a flow, the velocity of this effect can be calculated with varying frequency[24]. In the case where the mentioned forces are similar or higher than DEP force, alignment or particle separation will be compromised [15 - 20]. A high frequency signal (AC) will have this effect reduced, as the charged ions can't follow the fast change of polarization.

With the physics addressed, a macroscopic view of the process can be approached. Nanofabrication techniques allows the design of very small microelectrodes with gaps in the micrometer scale. It is found that the electrode gap must have around 0.8 the length of the corresponding nanowires for a maximum DEP force. [25] The usual DEP process aligns the nanowires on top of the electrodes with direct contact, when using higher voltages there's a risk of burning the bridging nanowires. The use of dielectric layer between the electrode and the deposition layer is found to prevent this issue. [26,27]

This has a few advantages over normal DEP process. First the electrochemical reactions between the particles and electrodes are eliminated, the electrothermal effects are reduced, the sample is not affected by fouling and the devices are chemically inert and robust. Also, the alignment electrodes may not be suitable for post-alignment building of systems, with a dielectric layer the desired interconnections can be built on top of the nanowires without any interference. [28]

1.3. Temperature sensor array

Humans have a variety of senses like hearing, sight, taste, smell or touch and technology has evolved to simulate each one of them with good success. Hearing can be linked to microphone and speakers, taste and smell to electronic tongue and nose, sight to cameras and touch to electronic skin (e-skin). Electronic skin requires a variety of sensors, such as humidity, pressure and temperature. In this work, V_2O_5 a material with high temperature coefficient of resistance (TCR) was used as the sensitive material for a flexible temperature sensor patch.

The aligned nanowires are used as a basic building block, each zone with high density alignment is used to fabricate a pixel. A pixel is the smallest component on a digital image, a spatial distribution of those pixels in a flexible patch allows a localized real-time analysis of the skin temperature.

The proposed temperature sensor has also a capability of being applied as bolometer, which is a device used for thermal imaging through infrared radiation (IR) usually with wavelengths between 8 μm to 12 μm. There are two types of infrared detectors, photon and thermal, photon detectors absorb radiation through the photon-electron interaction, where thermal detectors are based on the variation of electrical properties on the sensitive material with heating. In the last, there is no electron-photon interaction, the sensitive layer experiences heating from an absorbing layer that as large IR absorbance coefficient.

Different figures of merit are used to characterize the bolometer performance, responsivity, detectivity and TCR. The only approached characteristic was the TCR that is defined by Eq.9.

$$\alpha = \frac{1}{R}\frac{dR}{dT} \tag{9}$$

TCR value depends on the material type, metals have higher resistance with temperature (positive TCR), since resistivity depends on the drift speed of the electrons, which depends on the particle collisions. Higher temperature will increase the number of collisions between electrons and atoms resulting in lower drift speed and less current. On the opposite, semiconductors have negative TCR, as the resistance lowers with temperature. Higher temperature lowers the bandgap of the semiconductor leading to more free electrons, resulting in higher currents.

Each pixel of the array was addressed using a passive matrix. A reliability study of Via-bridges for passive matrix was published for the IEEE FLEPS Conference in Glasgow 2019, shown in Annex P.

1.3.1. Vanadium (V) Oxide

Vanadium oxide is known as having a high temperature coefficient of resistance with values around -4 $\%K^{-1}$ in thin films, making it highly desirable for thermal sensitive applications[32,33].

A precise study was previously made with V_2O_5 nanowires and fibres. The material crystallizes in orthorhombic layered structure of VO_5 square pyramids which are linked through the edges and corners between them, with lattice parameters of a = 11.54 Å , b = 3.571 Å and c = 4.383 Å [25,26].

Ultralong crystalline nanowires (80-120 nm diameter and cm long length) were synthesized by hydrothermal approach, with an individual nanofiber showing 0.5 S/cm at 300k and bandgap of 2.5 eV [31]. The conductivity occurs by polaron hopping between the V^{5+} and V^{4+} centres, it was concluded that with each V^{4+} there is an oxygen vacancy, so the ionization energy is the amount needed to remove the electron from this centre. The conductivity is anisotropic and greater in the axis where V-V distance is the shortest, closer cations result in a greater overlap of wave functions and the probability for tunnelling is higher, leading to higher conductivity [33].

2. Materials and Methods

2.1.Simulations

In order to simulate the electric field gradient on the fabricated electrodes the software Comsol® 5.4 was used, rendering the electric field strength (V/μm) and gradient (arrow surface). Both 2D and 3D images of the simulation were taken for both setups (PI and PVC), with the dimensions of the electrodes defined in section 2.2.1, a signal of 160 V and 100 kHz frequency. The 3D simulation was sliced at a depth of 100 μm on the water layer, where most of the nanowires will be attracted by the electric field. The gradient (arrow and cone surface) was plotted with the equations defined in (annex O) where the units for each square electric field gradient component ($x, y\ and\ z$) are $kg^2.m/(s^6.A^2)$. The constants used are defined in table 3 (Annex R). MatLab® was used to plot the real part of the Claussius-Mossoti factor. (Annex N)

2.2.Dielectrophoresis alignment

2.2.1. Electrode fabrication

The mask used has 4 arrays, each with different gap size (40, 50, 75, 100 μm), each array has approximately 1.5 cm side length with 15 columns, each with 15 small gaps, giving a total of 900 small gaps and a full size of 3 x 4.5 cm. Picture of the mask and corresponding sample is in Annex A.

Standard photolithography procedure was used for the fabrication of the electrodes. A 6 x 6 cm sheet of polyimide was cleaned for 9 min. in an ultrasonic bath with acetone, isopropanol alcohol (IPA) and reverse osmose (RO) water, each of them for 3 minutes. After cleaning and drying, a 4-inch wafer was used as a carrier for the clean polyimide. MicroChem Primer 80/20 was spinned on the substrate at 3000 rpm for 30 sec, followed by Microposit photoresist S1805 with same conditions. A soft-bake was made in a hotplate at 65 °C for 2 minutes. After spinning, the substrate was soaked in 1:1 solution of Microposit developer concentrate for 2 minutes, rinsed for 1 minute and finished with another soft-bake at 90 °C for 2 minutes. The substrate was then exposed to UV for 3 seconds with hard contact using the mask aligner SUSS Microtec MA6. After exposure, the substrate was baked again at 125 °C and developed with the same 1:1 Microposit solution for 2 minutes.

Before metallization the substrate was subjected to a O_2 treatment for 1 minute at 100 Watts power, to clean and improve the adhesion of the metal to the substrate. The metallization was made with e-beam evaporation through the Plassys MEB550S equipment, it was evaporated 10 nm of Nichrome followed by 140 nm of Gold. After metallization the sample was submersed in Microposit remover 1165 and left in a hot bath of 50 °C for at least 30 minutes, while it was periodically checked until the lift-off is successful.

Two photolithography recipes were used in this work, the first is detailed Annex P and the second is the one described above.

2.2.2. Preparation of NW suspension

Different concentrations were used along the work but the main solution used in the parameter study is explained here. Commercial Vanadium pentoxide nanowires were used from Novarials with lengths higher than 100 μm and diameter of 40 nm. 0.05 g of nanowire cluster was weight into 15 mL of DI water and stirred for 30 to 60 minutes at 350 rpm, until the clusters are reduced to very small agglomerates. More 15 mL of DI water was added to dilute the nanowire concentration and the mixture was ultrasonicated with Camsonix C575T to disperse the remaining clusters and break the nanowires into smaller lengths.

2.2.3. Design of container

The containers for the solution were designed to support the electrodes and load the nanowire solution. The first is a simple container with 3.5 cm width and 5 cm height with an opening of 6 mm and 2 legs that can be in an angled position. The second is a larger container with 7 cm width and 6 cm height with 10 cm opening. A carrier for the substrate was also designed. All the parts were designed in Solidworks 2018 and 3D printed in an Ultimaker S^5 with Easyprint PLA 2.85 mm material. The sketches are found in annex C.

2.2.4. Dip coating alignment

The alignment procedure combines the products of the 3 procedures described above. In top PVC alignment the electrodes are insulated with PVC using hot lamination technique, the alignment will be observed on top of this layer. In the backside polyimide alignment, the electrodes are insulated with Kapton tape and the alignment is going to be observed in the backside of the polyimide substrate, a schematic of both setups is found in annex B.

The first step is to connect 3 external wires to the pads with copper tape and silver conductive adhesive paint from RS pro. Then the substrate was fixed to a carrier that will transport the sample inside and out of the container. The solution is poured on the container, the electrodes submersed and an AC signal was applied with the signal generator Teledyne Lecroy wave station 3082, which was connected to an FLC electronics A400DI amplifier. After alignment the substrate was pulled out manually and the signal turned off. In the PVC-setup the small container was used. PI-setup was an upgraded version of the experiment where the substrate is fixed in a printed carrier that can be fixed to a motorized linear stage X-LSM050A from Zaber. In this setup the larger container was positioned below the carrier and filled with the nanowire dispersion. Annex D shows both alignment setups.

2.3. Characterizations

2.3.1. Morphological and elemental analysis

High resolution images were taken using scanning electron microscope (SEM) SU8240 from Hitachi. Nanowire alignment was analysed with GT Fiber software and the nanowire density by counting the amount of NW by the corresponding width. X-ray spectroscopy was performed on the same SEM equipment.

2.3.2. Optical microscopy

Two microscopes were used, the first is a Nikon Eclipse LV160ND and the second is a Leica M165C mounted on an optical table. These were mostly used for a macroscopic analysis of the aligned nanowires.

2.3.3. Thermo-electrical characterization

Thermal characterization of the sensor was performed with a hotplate as the heat source, the sample is fixed on a metal plate and connected to the Agilent 34461A 6.5-digit multimeter. For the contactless test the metal plate is positioned 20 cm away from the hotplate, where the sample is facing the hotplate and on top a beaker with water is placed. For the contact test the metal plate is placed on top of the hotplate. Temperature variation is 5 °C and 25 °C for contact and contactless test, respectively, where an IV curve is plotted with 2 minutes separation for each temperature step. The setup is shown in annex G.

3. Results and Discussion

3.1.Simulations

3.1.1. Clausius-Mossotti factor

The Clausius-Mossotti factor dependency of frequency is plotted in the fig. 2, both for long and short-axis of the nanowire. The long-axis component is dominant at low frequencies and lowers from 100 Hz to 1 MHz where the short-axis component will become dominant. The short-axis component is responsible to move the nanowires into the high-density field gradient zones (small gaps of the electrodes), so a better yield is expected when the short-axis becomes dominant over long-axis component which occurs with the increasing frequency.

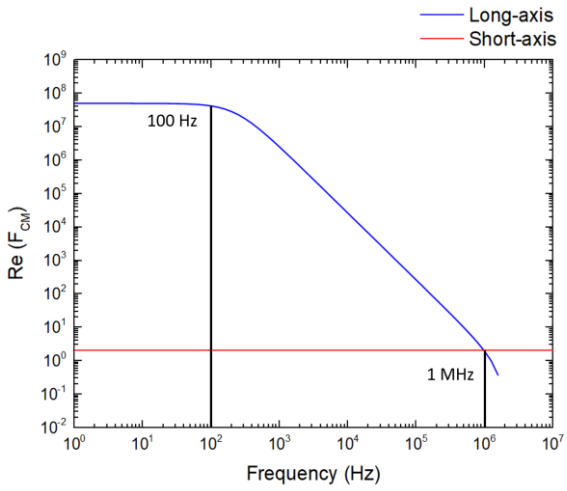

Figure 2 – F_{CM} plot with frequency for long and short axis of the V_2O_5 nanowire.

3.1.2. Electric-Field

With electric field gradient simulations through the material layers it is possible to better understand how strong the field is at certain depth and how the results compare to such values.

In Fig. 3 the contour lines represent the electric field strength around the gap zone, it has values of 0.1 close to the polyimide substrate and lowers to 0.06 V/µm at 100 µm above the gap, it is expected that nanowires within at least 200 µm will feel a strong enough attraction force. Comparing both PVC (Annex S) and PI setup (Fig.3), a slight decrease on the electric field strength is found with PVC. This occurs due to the change in dielectric properties between PVC/PI and the thickness of PVC that is 30 µm bigger than PI.

The electric field gradient can be observed with the arrow surface on both Fig.3 and 4, which is pointing towards the centre of the small gaps where the electric field is stronger.

Figure 4 represents the electric field strength and gradient distribution across the xy axis. The field is stronger where the gap is smaller as expected, but also between interconnects and electrode pairs which is not desirable. The electrode gap plays a very important role when a precise patterning and pixel separation is desired, the zones ranging from 0.02 to 0.05 V/µm will attract nanowires, as shown in Fig.11b. Optimizing the electrode geometry is of major importance to prevent deposition of nanowires in undesirable positions, zones where the simulation has light blue colour will still attract nanowires, the designing of new electrode geometries can be based on these simulations. An improved design of electrodes for isolated alignment pixels require a larger gap distance (dark blue) between the interconnections with

minimal spacings of 500 µm for 160 V, the alignment zones (red) have the gap defined by the nanowire length.

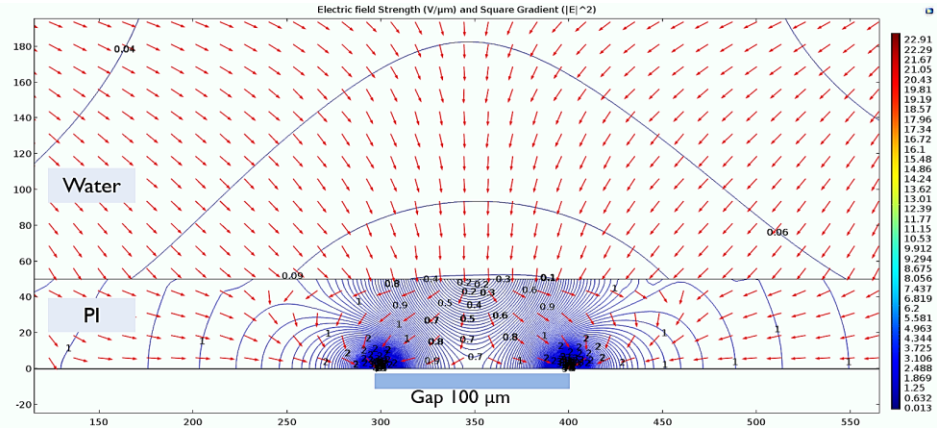

Figure 3 – 2D simulation of the square gradient (arrows) and electric field strength (contour) on the backside PI setup, bottom layer is PI and top layer is water.

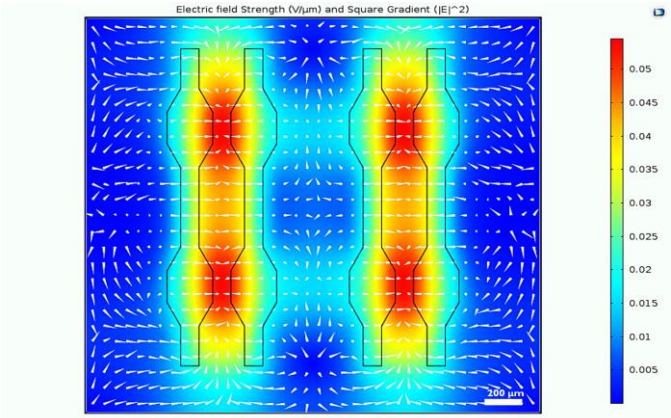

Figure 4 – 3D simulation of the square gradient (cones) and electric field strength (colors) on the backside PI setup, sliced at 100 µm on the water layer.

3.2.Dielectrophoresis Alignment

One crucial step for a successful alignment is the nanowire length relation to the gap size. Commercial nanowires have lengths up to the centimeter range and sonication was found to be effective in breaking the nanowires into smaller pieces suitable to the gap size of the microelectrodes, the length variation with ultrasound bath was studied with 0, 20 and 40 seconds. In Fig. 5 the lengths are considerable reduced due to sonication that will induce a bubble-jet and shock waves leading to nanowire fragmentation. The force applied on the structure is proportional to the nanowire length and reaches values above 100 GPa, while long nanowires will fracture due to bending, medium-smaller nanowires fracture due to tensile force. A more detailed study is made in [34].

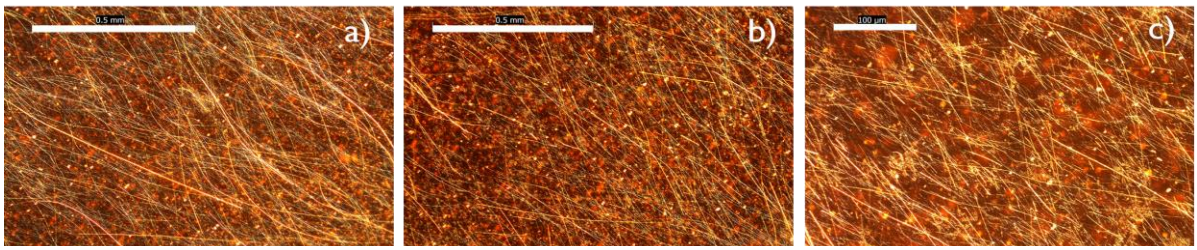

Figure 5 – Variation of nanowire length with different sonication times. **a)** 0 seconds. **b)** 20 seconds. **c)** 40 seconds.

3.2.1. Top-side PVC alignment

Microscope images were obtained using dark field mode, the substrate must be positioned in such way that the light is perpendicular to the nanowires, taking advantage of scattering effects for better visualization. The polyimide substrate is also fixed to a dark carrier to improve the contrast between the substrate and the nanowires.

The first step consisted in the optimization of the NW length and concentration with drop casting before optimizing the signal parameters. The first solution consists in 40 mL with unknown concentration of NW, Fig.6a, b, c represents a dried drop for different dilutions of the solution. Concentration will affect the alignment density, a higher concentration will result in a denser alignment but if the concentration is too high the nanowires will cover the entire substrate and templating does not occur.

The voltage study is shown in Fig.6 d, e, and f, in this experiment an air blow drier was used to aid the evaporation process of the drop through heating, this leads to an increase of the Brownian motion in the fluid which might overcome the DEP force that is very low at such voltages. With 25 V the DEP force is still not enough to attract nanowires into the desired position, although a small alignment can be observed.

Nevertheless, due to the use of a blow drier, the experiments for NW concentration and voltage investigation loses reliability due to the kinetic energy of the air hitting the drop.

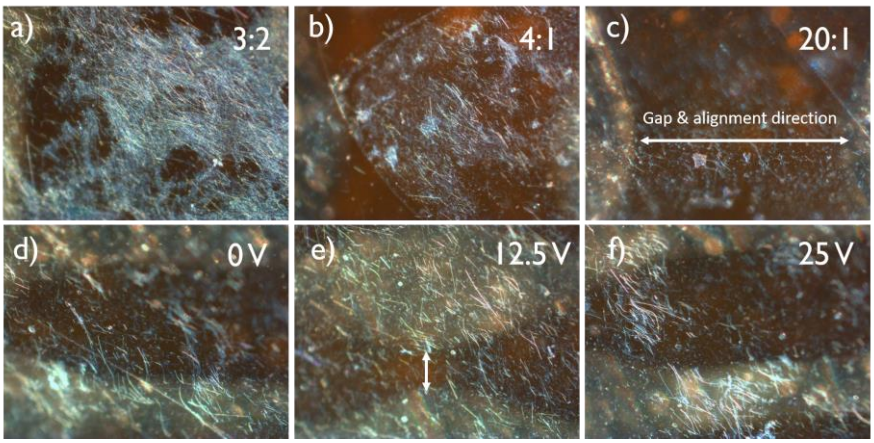

Figure 6 -Alignment experiments with 100 kHz frequency. **a, b, c)** Drop casting over PVC layer with different concentrations. **d, e, f)** Same setup with voltage variation.

After optimizing the concentration and the first voltage tests, follows the dip coating experiments which is the main objective of the work. To check how weak is the connection between the deposited NWs and the substrate, a drop was deposited and pipetted back after 10 min. As seen in figure 7 the NWs remained in the substrate as the suction force is not enough to pull out all the NWs from the substrate.

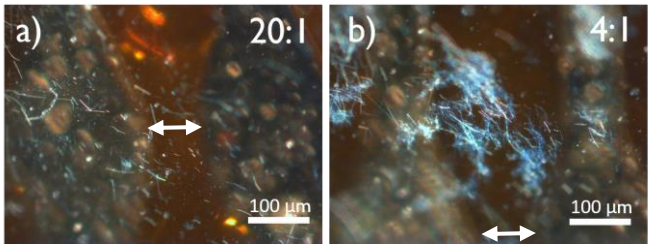

Figure 7 – a, b) Extracted drop with pipette after 10 min with different concentrations.

The first dip coating experiment was made with the container positioned vertically, the signal was applied for 30 minutes and the substrate was pulled out. It is important to note that the alignment direction is perpendicular to the withdrawal direction, during the withdrawal the flow will create a shear force on the nanowire perpendicular to the DEP alignment direction, misaligning the nanowires. [27], [35]

In Fig. 8a no alignment is present as the DEP force is not enough to attract the nanowires, withdrawal with field left on was also tested to maintain the DEP force applied during the pull-out but no improvement was observed (Fig.8b). The same experiment was made using the container with 60° angle (Fig. 8c), a slight improvement is observed but with very low quality. The voltage was increased to 50 V which leads to a higher DEP force resulting in a more noticeable alignment, figure 8d is an image of this experiment and reveals higher density but still a very poor alignment.

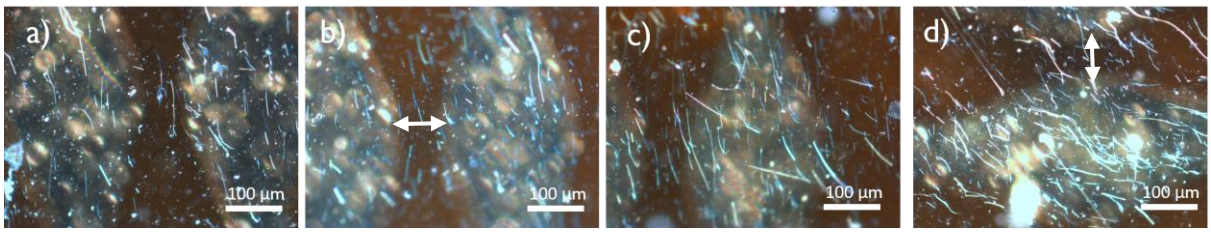

Figure 8 - Dip coating experiments. **a)** 12.5 V, 100 kHz, 25 minutes 6:4. **b, c)** Experiment with same conditions as a) with electric field on during pull-out and angled container, respectively. **d)** Experiment with 50 V, 100 kHz, 30 min, 4:1.

As low voltages and the flow shear force might be one of the principal causes preventing the alignment, a modification was made in the container to create a controllable flow extraction, a small hole around 2 mm was drilled on the bottom of the container and a very small tube with a 1 mm diameter opening was attached (Fig.9a). During the experiment a small binder clip is blocking the tube and it is removed after the experiment time, the solution is leaked onto a beaker drop by drop with an approximately flow of 0.33 mL/s.

An experiment with this setup was made with 25 min, 100 kHz, 4:1 concentration and higher voltage of 100 V, the results are shown in Fig. 9b, c. Increasing the voltage will increase the DEP force which increases the alignment quality, it is also observed the presence of clusters that are not desirable on the experiment, this is due to the reuse of the same solution that will have impurities and clusters of nanowires. The controllable solution extraction might have lowered the misalignment forces but its presence is still visible.

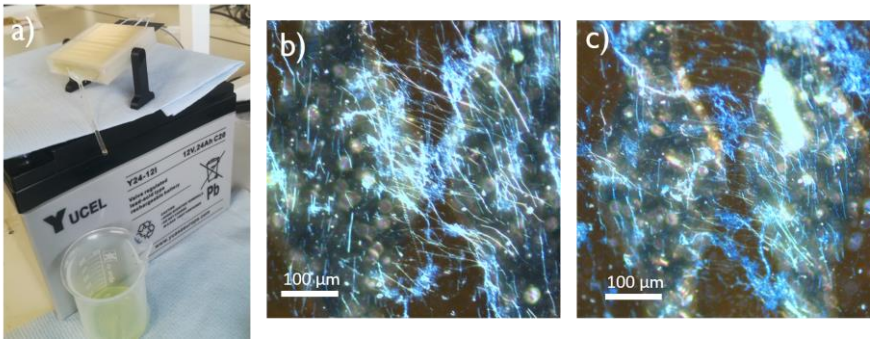

Figure 9 – a) Container with small tube attached and deposit beaker. **b, c)** Alignment experiment with controllable solution leak, using 100 V, 100 kHz and 4:1 for 25 minutes.

While raising the voltage the electrodes started to burn the substrate during the experiment, one explanation is that the increased voltage will lead to a localized joule heating. This heating melts the PVC layer and water leaks inside shorting the electrodes and burning the substrate (Annex I). This results in an unusable electrode delaying the progress, due to the time-consuming process of fabricating new electrodes.

However, raising the voltage to 180 V improved the alignment and density (Fig.10), the field strength is inversely proportional to the gap but as the voltage reaches such high values the field strength is going to be strong enough in gaps larger than 100 µm. Alignment starts to occur not only between the small gaps but also between the interconnections and electrode pairs (Fig. 10c), which was predicted by the

3D simulation (Fig.4). Also, in Fig.10c there is present a proof that the alignment is highly dependent on the relation between both DEP force and flow force direction, in the left side between the interconnects where DEP and flow forces are parallel the alignment and density is much higher than between the gaps, where the forces are perpendicular to each other.

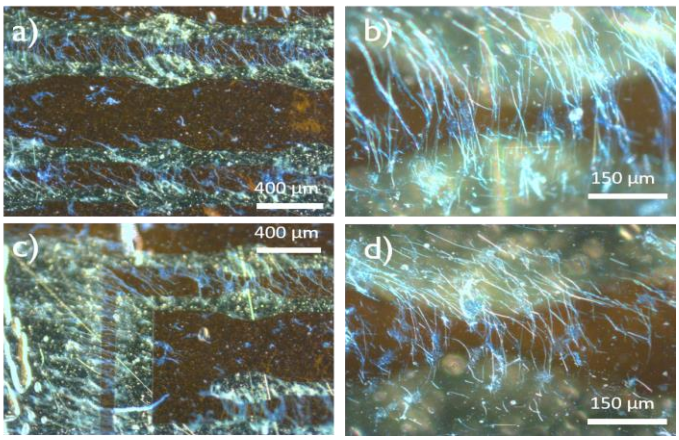

Figure 10 – **a)** Alignment experiment with 180 V, 100 kHz, 6:4 and 25 minutes. **a, b)** alignment zones on down left array (75 µm gap). **c, d)** Alignment on down right array (100 µm gap).

Here follows a summary of the outcomes from the experiments made with the top PVC alignment:

- ✓ Voltages over 150 V proved to be sufficient to create a strong electric field gradient on the surface of the dielectric PVC layer.
- ✓ The angle of the container and withdrawal with electric field on have small impact on the process.
- ✓ The drag force of the flow is an important factor affecting the alignment, the same way the flow can misalign the nanowires it can also create a force to align them if the alignment force is parallel to flow direction.
- ✓ High voltage burns the substrate and a replacement of the dielectric layer must be considered.
- ✓ Withdrawing the sample manually is not rigorous and a dangerous practice, a motor with micrometer resolution can be used to control the withdrawal and make the process automated without human handling.

3.2.2. Backside polyimide alignment

The backside polyimide alignment is an upgraded version of the whole configuration and process, taking into account the previous results. The changes from the previous setup are bulleted below:

- ✓ The PVC layer was replaced by Kapton tape to insulate the electrodes, alignment now occurs on the backside of the substrate through the polyimide layer in which the electrodes are deposited. (Annex B)
- ✓ The withdrawal step of the carrier substrate is done by a micrometer resolution motor.
- ✓ Real-time viewing of the alignment process was possible due to the use of an optical table microscope with a coupled camera.
- ✓ Fresh bottle of nanowires from the same supplier replaced the 2-year-old nanowires.

The solution used in Fig. 11a has 0.04g with 10 mL of DI water, without sonication the nanowire length is much higher than the gaps preventing any alignment from occurring. With more 10 mL and 30 sec of sonication the nanowires have lengths in the range of the gap dimension and alignment is observed (Fig.

11b). Fig.11e and f represent dried drops and the NW orientation is highly affected by the evaporation of the drop, also the coffee ring effect is clearly visible.

With 260 V the voltage reaches such high levels that the nanowires tend to align in the larger gaps between the electrode pair, one explanation for this might be that the dipole created on the nanowire will generate an electric field around the nanowire strong enough to attract other nanowires. Without a SEM image it is not possible to state a reliable conclusion, it might also be alignment of nanowires with lengths proximal to the larger gap size.[36]

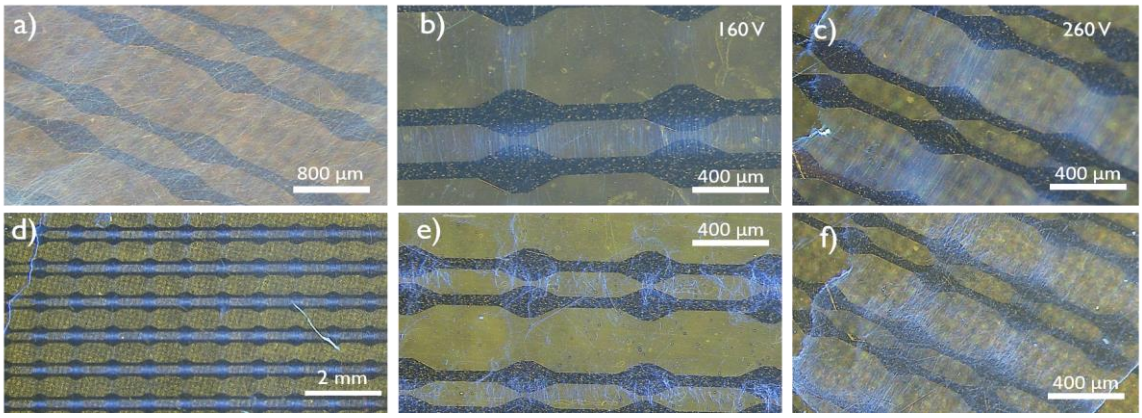

Figure 11 – a) Drop casting of 0.04 g in 10 mL without ultrasound treatment. **b, c)** Alignment with 160 V and 260 V after adding 20 mL and 30 sec of sonication. **d)** Image of the large-area alignment. **e, f)** Alignment post-evaporation of b) and c) images.

After optimizing the solution to the new setup with drop casting, the dip coating setup could be optimized. The first test was made with 260 V, 1 MHz and withdrawal speed of 100 µm/s (Fig.12a). The use of a very slow pull-out motion was expected to reduce the misalignment but the flow force is still present even with such a small speed.

The withdrawal step proved to have great impact on the process. The alignment and flow direction are perpendicular and leads to misalignment, with this, the sample was rotated 90° so the direction of alignment and drag force is parallel. The first experiment with the rotated substrate was made with 160 V, 100 kHz and 10 µm/s, the alignment clearly improved and the effect of the flow promoting the alignment is shown in Fig. 12b.

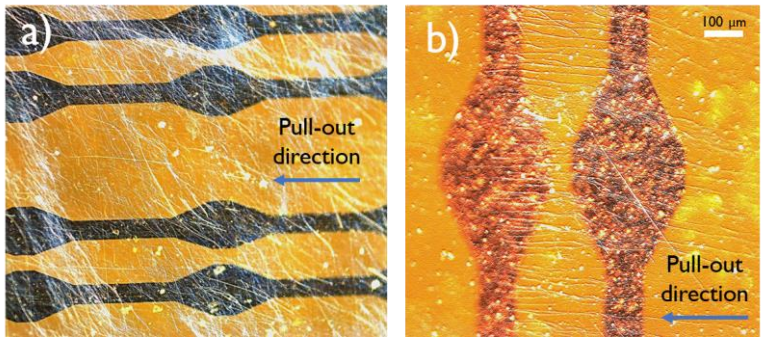

Figure 12 – a) Experiment with perpendicular flow and alignment direction. **b)** Experiment with parallel flow and alignment direction**.**

With the drag force of the flow issue fixed, a parameter study was made, to better understand how each variable influences the alignment and what is the combination in which the alignment and density is highest.

3.2.2.1. Submersion time

The time study in which the sample is submersed is present on Fig. 13, the experiment was conducted with 160 V, 100 kHz and a withdrawal speed of 100 µm/s. It is known that dielectrophoresis is a time dependent technique, more time results in more nanowires being attracted by the field and aligned between the gaps. In Fig. 13 the difference of density between 2 and 10 minutes is noticeable, with more time the density is higher but alignment is compromised.

During the video observations of a drop casting experiment with a video camera embedded in the microscope an interesting effect is observed. The alignment occurs in the first seconds, nanowires that are close to the gap will be instantly pulled towards the high-density field, however, nanowires that are more distant will take more time until they reach the high gradient zone and rapidly align. The misalignment present in Fig.13c can be explained with nanowires that are randomly moving on the solution through Brownian effect or buoyancy, these nanowires will move freely until they reach a zone where the gradient starts to create enough force to overcome the viscous force and pull the nanowires until they settle.

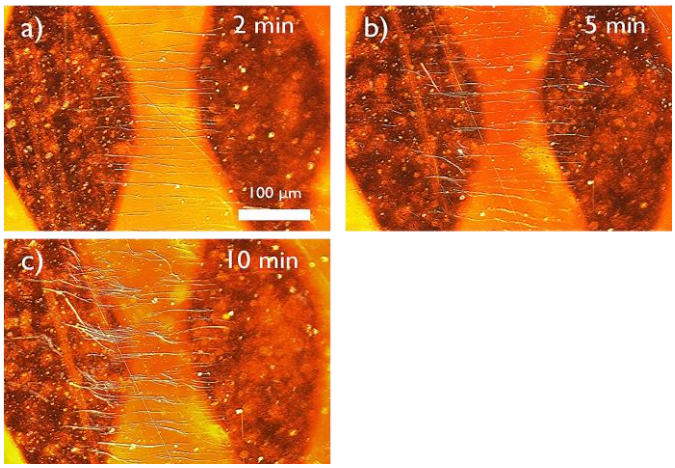

Figure 13 – Effect of submersion time on nanowire alignment with 160 V_{PP}, 100 kHz and 100 µm/s withdrawal speed.

3.2.2.2. Signal frequency

The signal frequency parameter study was made with the parameters fixed at 300 V_{PP}, 100 µm/s and 2 minutes inside the solution. With the increasing frequency it is expected through the simulations that the short-axis component dominates leading to a higher density of alignment. In Fig.16 this effect is clearly observed and at 1 MHz the alignment density is higher than 100 or 10 kHz, consistent with the simulation.

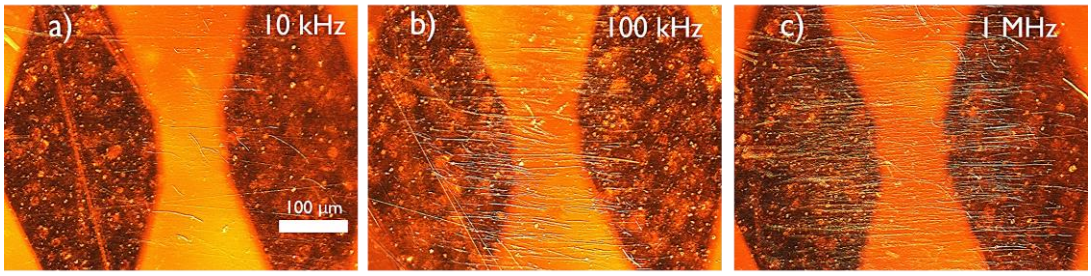

Figure 14 – Effect of frequency on nanowire alignment with 300 V_{PP}, 100 µm/s and 2 min. submersion time.

3.2.2.3. Applied V_{PP}

The first voltage study was made with 100 kHz and withdrawal at 100 µm/s after 2 minutes submersed in the solution. As expected, the change from 160 V to 300 V results in a denser alignment of nanowires, raising the voltage will also make the electric field reach higher radius (as seen in 2D field simulation) attracting more nanowires. With higher force the alignment is improved and the nanowires are

almost perfectly aligned with the field lines, also the density increases because the gradient in the gap is much higher and attracts more NWs to that zone.

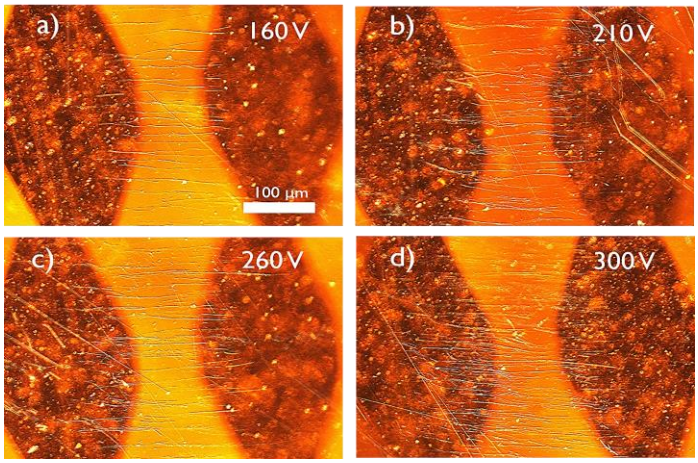

Figure 15 – Effect of voltage on nanowire alignment with 100 kHz, 100 µm/s and 2 min. of submersion time.

A second voltage study was made with the same conditions (100 µm/s and 2min. time) but with a higher frequency of 1 MHz. Comparing Fig. 14 and 15, the density is higher for all values of voltages using 1 MHz instead of 100 kHz. Also, the alignment density at 1 MHz increases with voltage due to higher DEP force but it does not have the significance that the frequency has on the process.

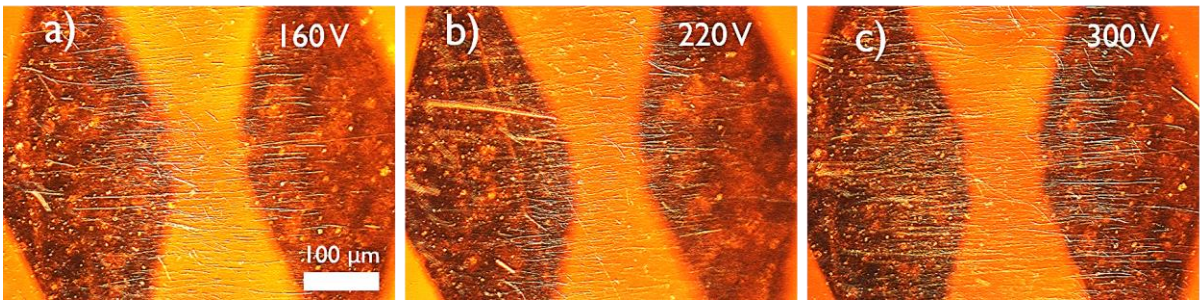

Figure 16 – Effect of voltage on nanowire alignment with 1 MHz, 100 µm/s and 2 min. of submersion time.

3.2.2.4. Withdrawal speed

The withdrawal speed study was made with 1 MHz, 300 V_{PP} and 2 min. of submersion. Raising the pull-out speed proved to have low impact on the alignment and density of the nanowires, through microscope images the differences are minimal and it's not possible to make a reliable conclusion. On all 3 speeds the density and alignment is good, the drag force will occur post-alignment and an improve can be expected on higher speeds as the drag force will generate more force to align the nanowires.

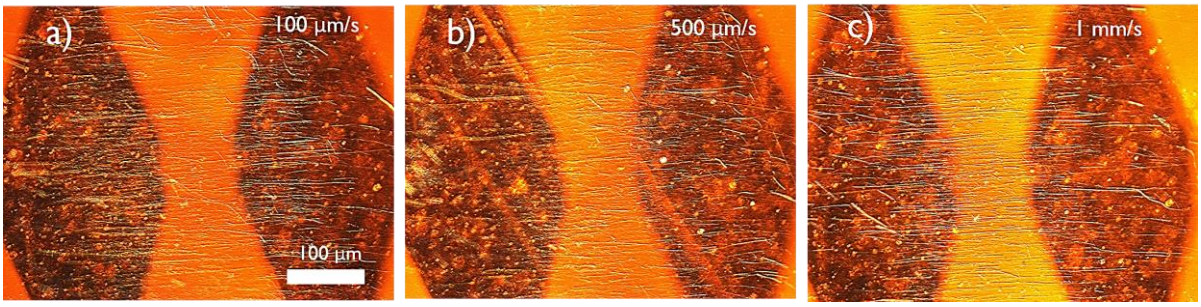

Figure 17 – Effect of withdrawal speed with 300 V_{PP}, 1 MHz and 2 min. submersion time.

In order to have a more precise study of the withdrawal speed influence, the conditions were kept the same (1 MHz, 300 V_{PP}) and the carrier has a continuous movement inside and out instead of stopping 2

min before pull-out. Basically, the alignment will occur by continuously aligning nanowires from different zones as the substrate moves through the solution. This will also create a flow on the container moving nanowires that may approximate the surface and get pulled by the field. With a higher speed (Fig. 18b) the density is less than lower speeds because there is not enough time to attract the nanowires in the vicinities, also, lower speeds result in more time inside the solution leading to a denser alignment.

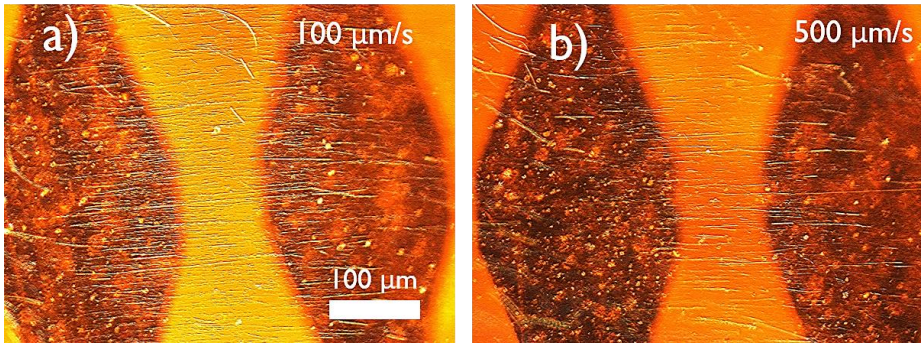

Figure 18 – Effect of withdrawal speed with continuous movement using 300 V_{PP}, 1 MHz and 2 min. submersion time.

Summing up the parameter study, the best combination for high density alignment is 300 V_{PP}, 1 MHz and a continuous movement down and up at 100 µm/s. It is important to note that in order to have higher density the same sample can be dipped more than one time. The large-scale alignment was obtained with the optimization of all the factors involving the process, these parameters were optimized to the characteristics of the system (electrode geometry, gap length, NW length, diameter and both particle and medium dielectric properties).

In order to make the whole process (electrode fabrication, alignment and device fabrication) easier, low-cost and more customizable, it was proposed the use of a double-sided tape to make the electrode substrate and the alignment substrate two different parts. Using a very thin double-sided tape (5 µm) from Nitto the electrode substrate can be fixed to another substrate that will be peeled-off after the alignment process. This can be used with different combinations of substrates. The concept was proved using glass substrate with electrodes and the tape where only one PET liner is removed, leaving the top PET (28µm thickness) on the tape which will act as the alignment substrate. This structure is shown in Fig.19a, Fig.19 b and c represent the aligned NW in pre and post peel-off, respectively.

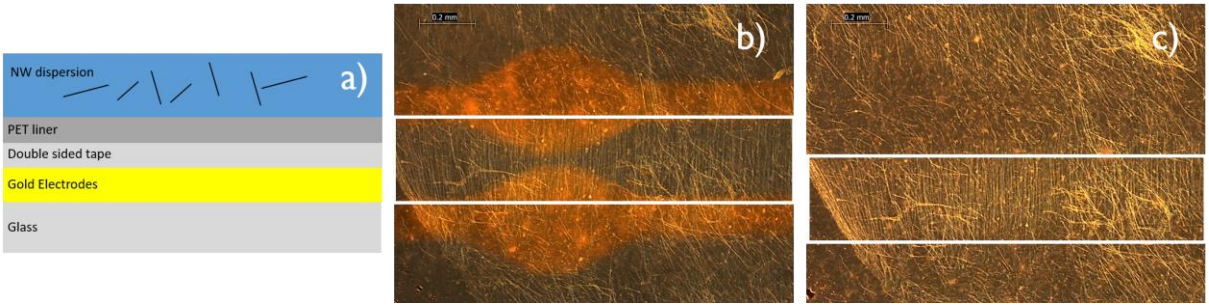

Figure 19 – a) Structure with double-sided tape configuration. **b)** Drop casted alignment (inside white rectangle) on top of the PET film on glass substrate. **c)** PET film after glass peel-off without electrodes on the backside.

3.3. Aligned Nanowires characterization

3.3.1. Optical characterization of aligned nanowires

PI backside alignment with 3-time dipping is shown in Fig.20 with the respective SEM images. The density was calculated to be 14 NW/μm with 0.96 alignment, where 1 is a perfect alignment. Comparing the microscope image with the SEM image, the number of nanowires aligned are much higher than it looks in the microscope images used in the parameter study, nanowires with smaller diameters become too small and it is not possible to see them under a normal microscope.

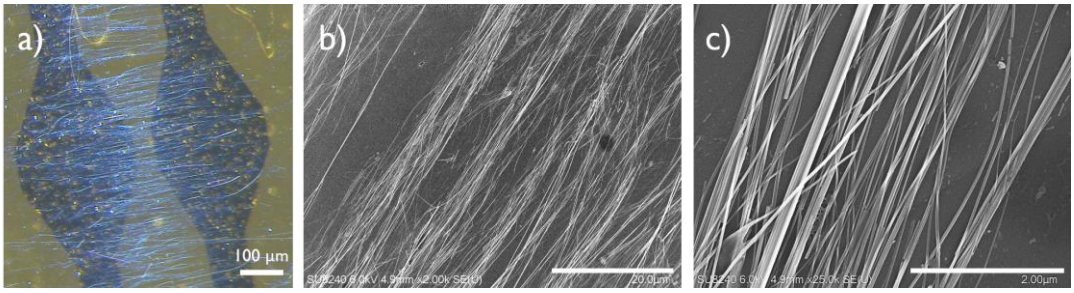

Figure 20 – Backside alignment of nanowires. **a)** Alignment with 160 V_{PP}, 100 kHz, 100 μm/sec with 3-time dipping. **b,c)** Aligned nanowires on the backside of PI with 2 different magnifications.

3.3.2. Energy dispersive spectroscopy

The EDS element spectrum reveals peaks in carbon prevenient from the carbon tape, vanadium and oxygen (Annex Q). The weight and atomic composition without carbon is shown in table 2, nanowires from the new batch have a V:O relation similar to 2:5, consistent with the V_2O_5 structure.

Table 1 - EDS atomic and mass weight.

	Mass (%)	**Atomic (%)**
Vanadium	48.52	22.84
Oxygen	51.48	77.16

3.3.3. Pixel lift-off characterization

In order to address each pixel, two pads were patterned with lithography with the nanowires bridging both (Fig.21), the 3-step process of spinning, development and lift-off is shown in figure 21 a, b, c, in each step a percentage of nanowires is lost, decreasing the density and thus the performance per pixel of the device. It is highly desirable to maintain the initial density of nanowires to have similar high performances between pixels.

Lithography is a very harsh process for the nanowires that are only deposited on the PI surface, fixed by weak Van der Walls forces. One solution to improve the adhesion between the nanowires and substrate is annealing them at high temperature of 180 °C for 30 minutes, and, if possible, the use of a N_2 furnace to prevent oxidation on the material.

SEM images after the lift-off are shown in Fig.21d, e, and f, revealing that the nanowires have a coating after processing, this can be justified by a poor lift-off, meaning that a part of the photoresist remains in the nanowire surface.

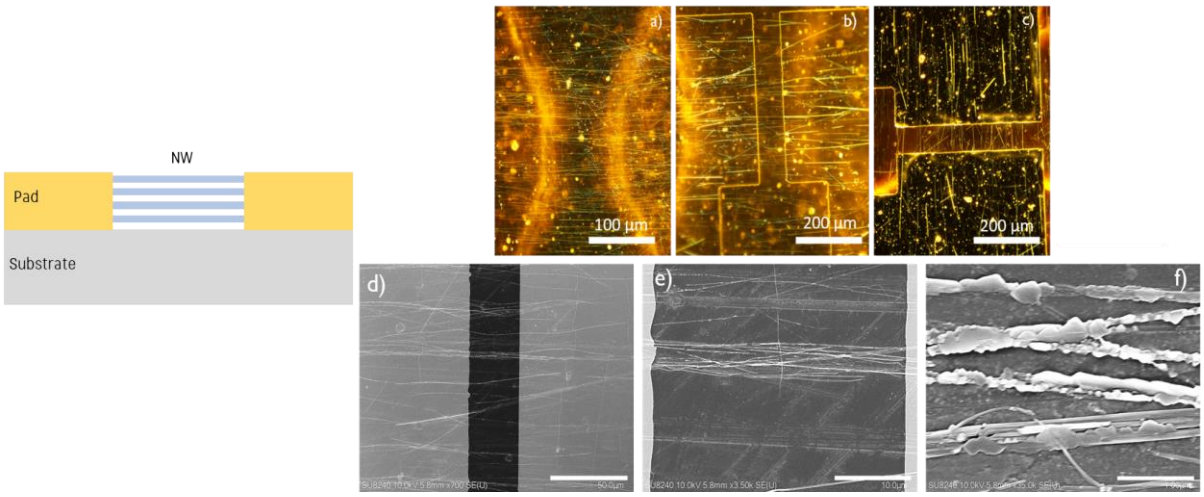

Figure 21 – Cross-section of the fabricated pixels. **a)** Aligned nanowires between electrode gap (backside) with photoresist. **b)** Photoresist developed pads. **c)** Lifted-off electrode pads with nanowire bridge. **d, e, f)** SEM image of lifted-off sample with increasing approximation.

3.3.4. Electrical characterization of single V_2O_5 pixel

An IV curve of a lifted-off pixel was made, the nanowires belong to the old batch and the corresponding pixel is in figure 22b. In a closer look at the image approximately 5 NW are bridging the pads, the resultant resistance is 12.2 MΩ. Such high value is due to the low density of nanowires but through the SEM image residues of photoresist are observed, this will raise the contact resistance between the pads and nanowires, resulting in a higher resistance.

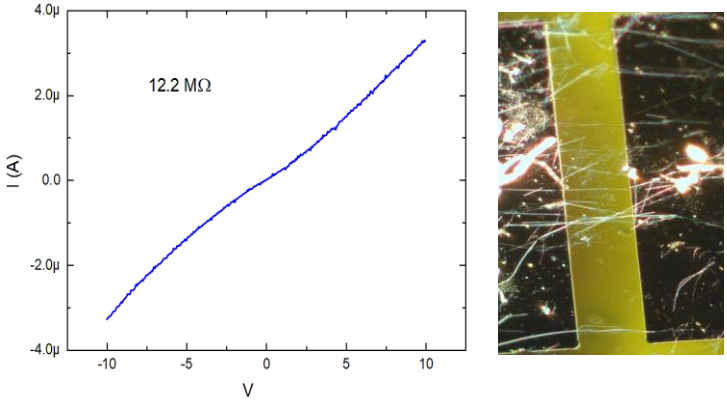

Figure 22 – IV curve of aligned nanowires after lift-off with the corresponding analysed pixel.

3.4. Temperature sensor array

3.4.1. Passive Matrix fabrication

The temperature sensor pixels were addressed using a passive matrix with a Via-bridge, the schematic is presented in figure 23. The alignment electrodes array has 900 small gaps which result in 900 independent pixels of thermal sensitive nanowires (V_2O_5). The reliability of the Via-bridges was verified by bridging the pixel pads followed by an electro-mechanical test on one column to row path, the results are shown in the submitted conference paper (Annex P). The full device with the thermal sensitive pixels and passive matrix addressing was not reached due to time limitations.

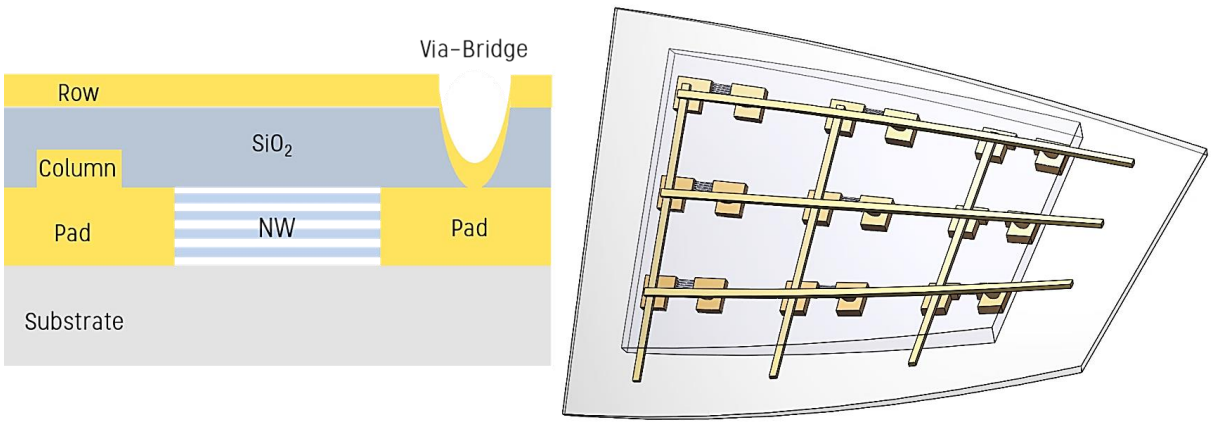

Figure 23 – Cross-section and 3D model of the passive matrix addressed nanowire pixels.

During the Via-bridge fabrication a problem occurred with the lift-off process of the top row lines, the use of ultrasound which was supposed to help the Au lift-off also removed the gold at zones where the SiO_x is on top of the polyimide (Fig.24d). This can be explained by the thickness of the depositions, the pad and column have 100 nm, the insulating layer 500 nm and the row 150 nm. The zone of the row that is on top of the polyimide has a step of 100 nm comparing to the zones on top of the pad or column, the ultrasound force was enough to remove this layer that is in a fragile conformation.

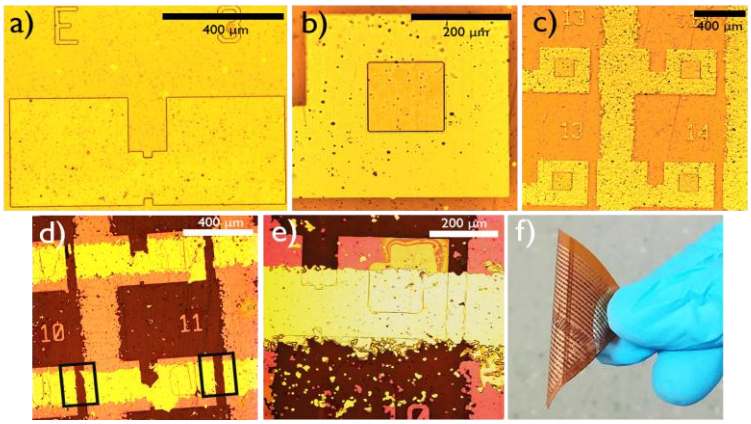

Figure 24 – a) Developed photoresist of bridged pads. **b)** Developed Via-hole photoresist. **c)** Deposited column on the left-side pad and developed Via-hole in the right-side pad. **d)** Top row deposition with lift-off problem. **e)** Fixed row line on top of the Via-hole. **f)** Image of the fabricated flexible sample.

3.4.2. Thermal characterization

The thermal characterization was made with the new nanowires, the pad deposition with the bridging nanowires revealed issues leading to low density of nanowires. Due to this low density, the thermal characterization was made with aligned nanowires on top of the alignment electrodes, using them as interconnections. The IV curves correspond to the alignment made across the whole array, short circuiting the electrodes everywhere, shown in annex L. Through SEM image of the characterized sample (Fig. 25), a NW density of 9 NW/µm was calculated.

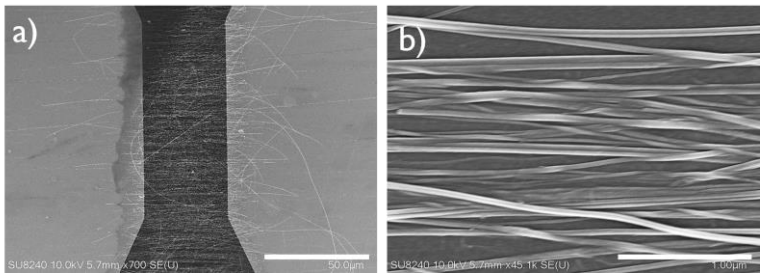

Figure 25 – a) SEM Image of alignment on top of the electrode. **b)** Approximation of the aligned nanowires.

The setup used for contactless experiment is very simple and it is not reliable for bolometer characterization, for a proper characterization the setup must comprise a vacuum chamber, IR source (laser or blackbody emitter) and a chopper for time response study.

TCR was obtained by plotting the curves of Fig. 26 with resistance variation to the initial resistance and the temperature variation, by fitting the obtained curves the TCR is extracted through the slope (Annex M), these results are shown in table 2.

Contact setup has a higher TCR than contactless (-0.97 $\%K^{-1}$), in contact setup the metal plate is touching the hotplate and there is heat transfer by conduction through the plate to the substrate and the NWs, the response is linear with the variation of temperature.

In contactless setup the heat transfer is due to radiation and reached a reasonable TCR of -0.1 $\%K^{-1}$, here the sensitive material (V_2O_5 NW) is in contact with 3 different materials, polyimide, PVC and gold, these will act as absorbents of IR radiation heating up and increasing the temperature of the NWs. Also, the size of the gold interconnections is a major conductive heat absorber that will influence the temperature of the NWs. Usually, in a microbolometer a chamber is etched below the sensitive layer in which a metal layer is deposited to reflect the infrared radiation back to the NWs, however, applying this on the used system is not an easy and straightforward process.

It is worth mentioning that Vanadium pentoxide is not biocompatible and needs to be isolated, this was made with lamination of PVC on top of the nanowires. Also, the lamination partly reduced the resistance as the nanowires are pressed against the electrodes, raising the contact area.

Table 2 - TCR (% K^{-1}) of contact and contactless setup.

	TCR (% K^{-1})
Contact	-0.977
Contactless	-0.108

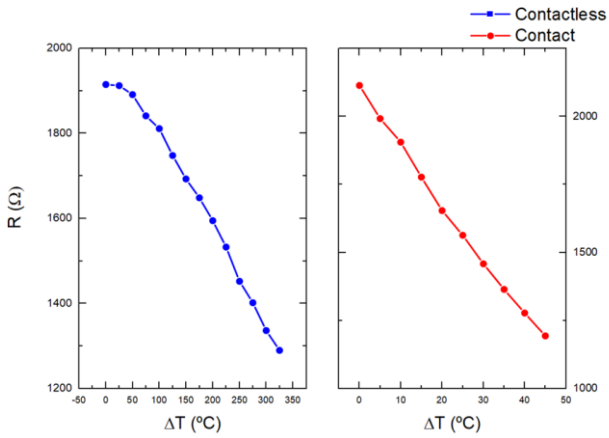

Figure 26 – Thermal characterization of Vanadium Pentoxide nanowires in contactless and contact setup, with the corresponding resistance and temperature variation.

4. Conclusions and Future directions

4.1.Conclusions

In this work the main objective was the large-area alignment of nanowires on flexible substrates through dielectrophoresis technique.

The simulations of the electric field strength and gradient proved to be precise with the conducted experiments, the gradient created with the gap size/voltage relation is important for a precise localized deposition.

The first dip coating experiments were made with voltages under 100 V and frequency of 100 kHz where no alignment was observed, even with a few variations such as, withdrawal with electric field on and angled container to minimize gravitational forces. The drag force created by the flow proved to be one of the most important aspects along with the voltage applied. Using voltages over 100 V and flipping the substrate to make the alignment and withdrawal direction parallel enabled the large-scale alignment of nanowires.

Dielectrophoresis alignment through an insulting layer is a viable process although it requires high voltages for a high yield in a dip coating system. The thickness between the electrode and the alignment zone must be the lowest possible to prevent the use of very high voltages that may damage the electrodes or the substrate.

The video capture of nanowire alignment showed that higher voltages and 1 MHz comparing to 100 kHz frequency led to a much faster alignment, also, the nanowires first rotate according to the field direction and then translate to the high gradient zones, the alignment process occurs in a few seconds after the application of the electric field. Higher frequencies revealed higher alignment density as the radial component of the Clausius Mossotti factor became dominant over the length component of the nanowire.

There are a few parameter relations for an optimized dip coating DEP alignment. The nanowire length and gap size are relevant in the electrode design, which can be predicted with Comsol simulations. The liquid in which the desired nanowire material is dispersed must be carefully picked through the dielectric constants and analysed with the Clausius-Mossotti simulation. To finish, the AC signal and withdrawal speed must be optimized according to the last two relations for a uniform large-scale alignment. SEM images of aligned nanowires on the backside revealed a 15 NW/μm with 96% alignment.

The second part of the work concerns the pixel fabrication with the nanowires as active component, the aligned nanowires might need a thermal treatment before the lithography steps to promote adhesion to the substrate and prevent any loss of nanowire density.

Thermal characterization of contact setup and contactless revealed a TCR of 0.97 and 0.1 $\%K^{-1}$, respectively. Contact setup has higher TCR as the heat transfer occurs faster through conduction than heating by IR radiation at 20 cm.

The main objective of aligning nanowires in a large-area on a flexible substrate was assured and preliminary work to achieve secondary objectives, such as pixel and passive-matrix fabrication for temperature sensing patch, have been started, nevertheless more work needs to be developed. During the 6 months period length of the thesis, a conference paper regarding the reliability of Via-bridges for flexible electronics was submitted for the IEEE FLEPS conference, Glasgow 2019 (Annex P).

4.2. Future directions

Due to this work large-scale integration of nanowires in a conformal and localized disposition on flexible substrates is one step closer to reality, the design of emerging applications for a variety of fields is possible but still some parameters need to be optimized and tuned-up according to the materials used.

A study with different materials and different gap size could reveal the influence of the voltage/gap size relation for optimal alignment. The electrode design is of extreme importance and is dependent on the nanowire length, Comsol simulations proved to be reliable and future designs can be based on these simulations.

With the reusable electrode concept using the double-sided tape a roll-to-roll application can be approached, also, only the nanowires that are in the proximities of the field are attracted, to improve the density of alignment a continuous flow could transport the nanowires to these zones. However, this flow should not be strong enough to overcome the DEP force.

The lift-off process is leaving residues of photoresist on the nanowires, more time of lift-off or a very thin layer can be deposited on top of the nanowires to prevent direct contact with the resist.

Thermal characterization of the array must be made under a reliable setup with vacuum chambers, IR emitter and choppers for response characterization.

Furthermore, with the DEP technology optimized the use of different materials, electrode configurations, substrates and a roll-to-roll process enables the possibility of fabricating devices for a wide range of flexible applications with the use of 1D nanostructures.

Bibliography

[1] K. Takei *et al.*, "Nanowire active-matrix circuitry for low-voltage macroscale artificial skin," *Nat. Mater.*, vol. 9, no. 10, pp. 821–826, 2010.

[2] Z. Li and Z. L. Wang, "Air/liquid-pressure and heartbeat-driven flexible fiber nanogenerators as a micro/nano-power source or diagnostic sensor," *Adv. Mater.*, 2011.

[3] K. Chen *et al.*, "Printed Carbon Nanotube Electronics and Sensor Systems," *Advanced Materials*. 2016.

[4] K. H. Tsui *et al.*, "Low-cost, flexible, and self-cleaning 3D nanocone anti-reflection films for high-efficiency photovoltaics," *Adv. Mater.*, 2014.

[5] K. Jain, S. Member, M. Klosner, and M. Zemel, "Flexible Electronics and Displays : Lithography and Photoablation Processing Technologies for High-Throughput Production," *Technology*, vol. 93, no. 8, 2005.

[6] J. Perelaer *et al.*, "Printed electronics: The challenges involved in printing devices, interconnects, and contacts based on inorganic materials," *J. Mater. Chem.*, 2010.

[7] B. Bhushan, *Handbook Springer of Nanotechnology*. 2013.

[8] J. Sarkar, G. G. Khan, and A. Basumallick, "Nanowires: Properties, applications and synthesis via porous anodic aluminium oxide template," *Bull. Mater. Sci.*, vol. 30, no. 3, pp. 271–290, 2007.

[9] N. S. Mohammad, "Understanding quantum confinement in nanowires: Basics, applications and possible laws," *J. Phys. Condens. Matter*, vol. 26, no. 42, 2014.

[10] W. T. Navaraj *et al.*, "Nanowire FET based neural element for robotic tactile sensing skin," *Front. Neurosci.*, vol. 11, no. SEP, p. 501, 2017.

[11] D. Zhang *et al.*, "Synthesis of ultralong copper nanowires for high-performance transparent electrodes," *J. Am. Chem. Soc.*, vol. 134, no. 35, pp. 14283–14286, 2012.

[12] Z. Liu, J. Xu, D. Chen, and G. Shen, "Flexible electronics based on inorganic nanowires," *Chemical Society Reviews*. 2015.

[13] B. Su, Y. Wu, and L. Jiang, "The art of aligning one-dimensional (1D) nanostructures," *Chemical Society Reviews*. 2012.

[14] L. Jiang, H. Dong, and W. Hu, "Controlled growth and assembly of one-dimensional ordered nanostructures of organic functional materials," *Soft Matter*, vol. 7, no. 5, pp. 1615–1630, 2011.

[15] H. Dai, R. Ding, M. Li, J. Huang, Y. Li, and M. Trevor, "Ordering Ag nanowire arrays by spontaneous spreading of volatile droplet on solid surface," *Sci. Rep.*, vol. 4, no. c, pp. 1–5, 2014.

[16] H. A. Pohl, "The motion and precipitation of suspensoids in divergent electric fields," *J. Appl. Phys.*, 1951.

[17] R. Pethig, "Dielectrophoresis: Status of the theory, technology, and applications," *Biomicrofluidics*, vol. 4, no. 2, 2010.

[18] K. Kendall, *Electromechanics of particles*, vol. 89, no. 2. 1996.

[19] R. Pethig, "Dielectrophoresis: Status of the theory, technology, and applications," *Biomicrofluidics*, 2010.

[20] "Ac electrokinetics: A review of forces in microelectrode structures," *J. Phys. D. Appl. Phys.*, vol. 31, no. 18, pp. 2338–2353, 1998.

[21] A. Ramos, Ed., *Electrokinetics and Electrohydrodynamics in Microsystems*. Vienna: Springer Vienna, 2011.

[22] R. Venkatesh, S. Kundu, A. Pradhan, T. P. Sai, A. Ghosh, and N. Ravishankar, "Directed Assembly of Ultrathin Gold Nanowires over Large Area by Dielectrophoresis," *Langmuir*, vol. 31, no. 33, pp. 9246–9252, 2015.

[23] S. Raychaudhuri, S. A. Dayeh, D. Wang, and E. T. Yu, "Precise semiconductor nanowire placement through dielectrophoresis," *Nano Lett.*, vol. 9, no. 6, pp. 2260–2266, 2009.

[24] A. W. Maijenburg *et al.*, "Dielectrophoretic alignment of metal and metal oxide nanowires and nanotubes: A universal set of parameters for bridging prepatterned microelectrodes," *J. Colloid Interface Sci.*, vol. 355, no. 2, pp. 486–493, 2011.

[25] Y. Liu, J. H. Chung, W. K. Liu, and R. S. Ruoff, "Dielectrophoretic assembly of nanowires," *J. Phys. Chem. B*, vol. 110, no. 29, pp. 14098–14106, 2006.

[26] X. Wang, K. Chen, L. Liu, N. Xiang, and Z. Ni, "Dielectrophoresis-based multi-step nanowire assembly on a flexible superstrate," *Nanotechnology*, 2018.

[27] M. Collet *et al.*, "Large-scale assembly of single nanowires through capillary-assisted dielectrophoresis," *Adv. Mater.*, vol. 27, no. 7, pp. 1268–1273, 2015.

[28] L. Liu, K. Chen, N. Xiang, and Z. Ni, "Dielectrophoretic manipulation of nanomaterials: A review," *Electrophoresis*, vol. 40, no. 6. pp. 873–889, 2019.

[29] W. B. Fu, G. L. Shang, X. X. Gong, L. De Zhang, and G. T. Fei, "Preparation of large scale and highly ordered vanadium pentoxide (V2O5) nanowire arrays towards high performance photodetectors," *J. Mater. Chem. C*, vol. 5, no. 6, pp. 1471–1478, 2017.

[30] K. W. Sun, "Transport properties of single vanadium oxide nanowire," *Phys. Procedia*, vol. 22, no. 2010, pp. 8–13, 2011.

[31] T. Zhai *et al.*, "Centimeter-long v2O5 nanowires: From synthesis to field-emission, electrochemical, electrical transport, and photoconductive properties," *Adv. Mater.*, vol. 22, no. 23, pp. 2547–2552, 2010.

[32] K. Y. Pan and D. H. Wei, "Optoelectronic and electrochemical properties of vanadium Pentoxide Nanowires synthesized by vapor-solid process," *Nanomaterials*, vol. 6, no. 8, 2016.

[33] J. Muster *et al.*, "Electrical transport through individual vanadium pentoxide nanowires," *Adv. Mater.*, vol. 12, no. 6, pp. 420–424, 2000.

[34] H. Dai, T. Y. Wang, and M. C. Li, "Spotlight on ultrasonic fracture behaviour of nanowires: Their size-dependent effect and prospect for controllable functional modification," *RSC Adv.*, vol. 6, no. 76, pp. 72080–72085, 2016.

[35] K. Oh, J. H. Chung, J. J. Riley, Y. Liu, and W. K. Liu, "Fluid flow-assisted dielectrophoretic assembly of nanowires," *Langmuir*, vol. 23, no. 23, pp. 11932–11940, 2007.

[36] M. Sam, N. Moghimian, and R. B. Bhiladvala, "Field-directed chaining of nanowires: Towards transparent electrodes," *Mater. Lett.*, vol. 163, pp. 205–208, 2016.

[37] Professionalplastics.com. (n.d.). [online] Available at: https://www.professionalplastics.com/professionalplastics/ElectricalPropertiesofPlastics.pdf [Accessed 14 Sep. 2019].

[38] Mit.edu. (n.d.). *Gold properties*. [online] Available at: http://www.mit.edu/~6.777/matprops/gold.htm [Accessed 14 Sep. 2019].

Annex

Annex A – Electrode array mask (left) and the corresponding nanofabricated sample on polyimide.

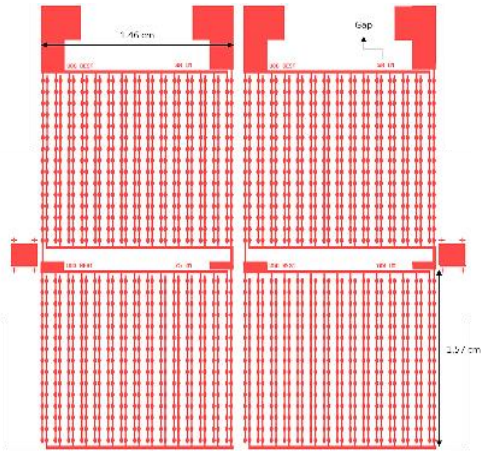

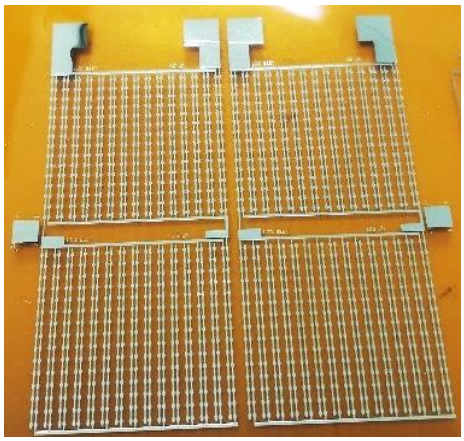

Annex B – PVC setup (left) and PI setup (right).

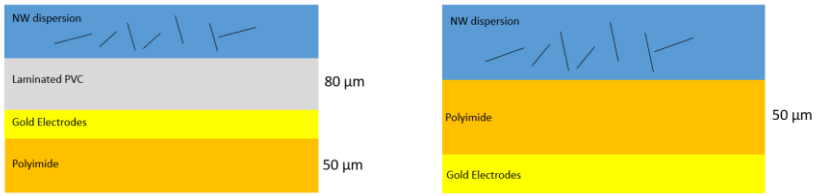

Annex C - Model of PVC setup container (Left), PI setup container (middle) and PI setup substrate carrier (right).

Annex D – Array connected with external wires (left), dip coating of PVC setup (middle) and motorized dip coating of the PI setup (right).

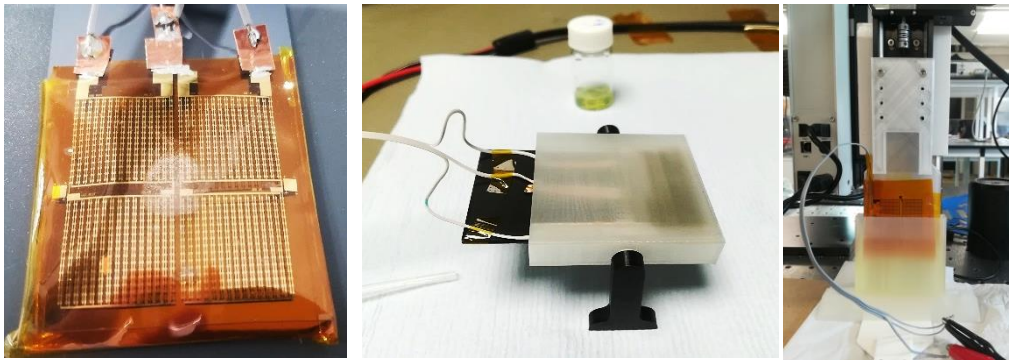

Annex E – Passive matrix with plugless Via-bridge schematic model.

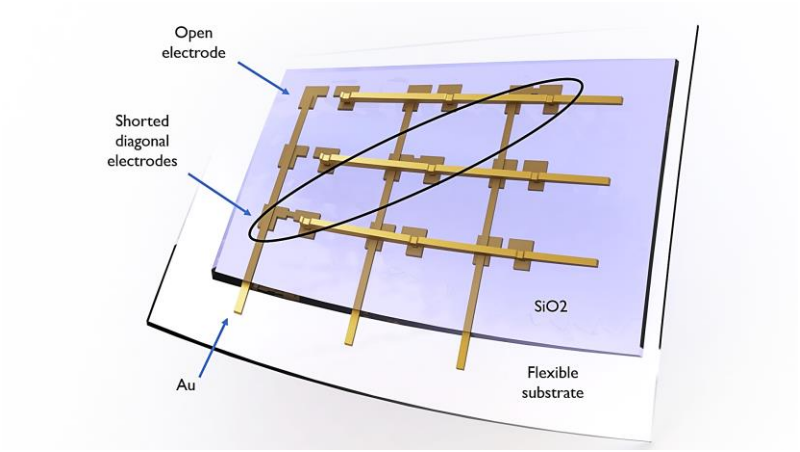

Annex F - Electrode and passive matrix schematic dimensions.

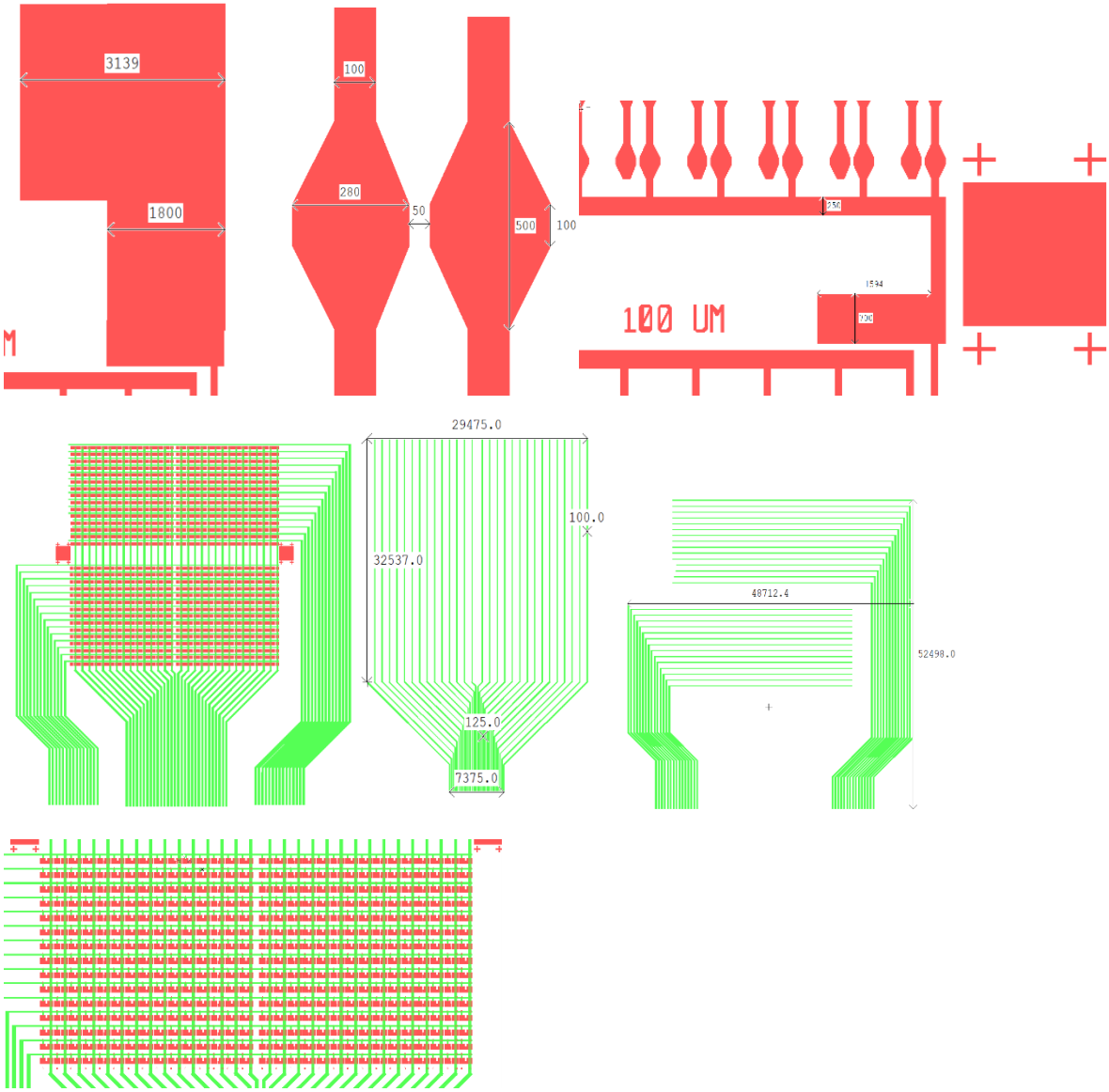

Annex G – Piece of metal with fixed sample (left), Contactless setup with beaker cooling the metal piece (centre) and contact setup.

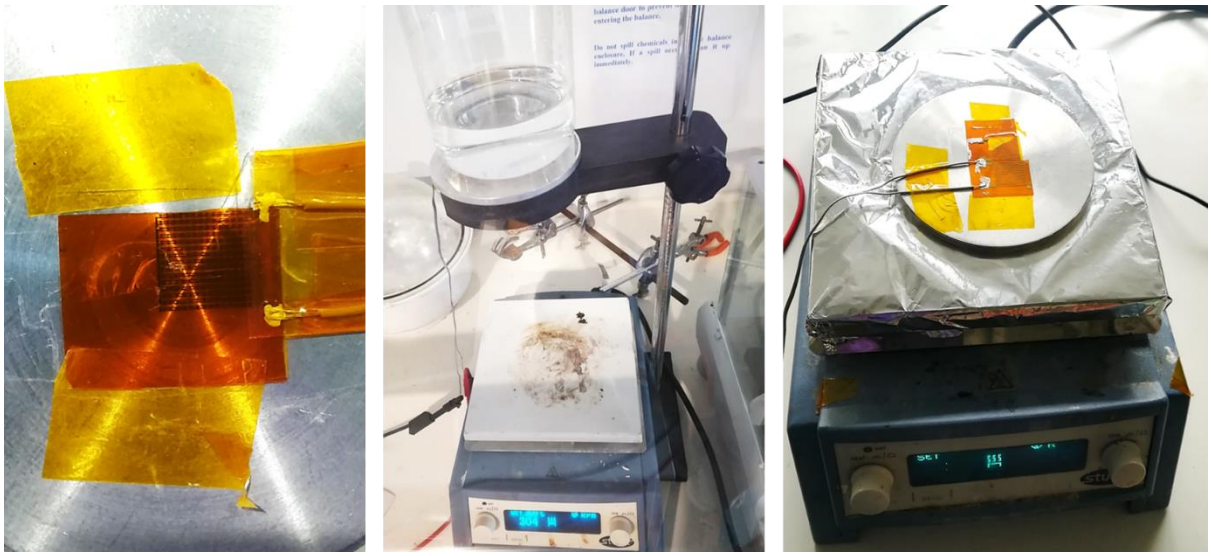

Annex H – Electro-mechanical test setup.

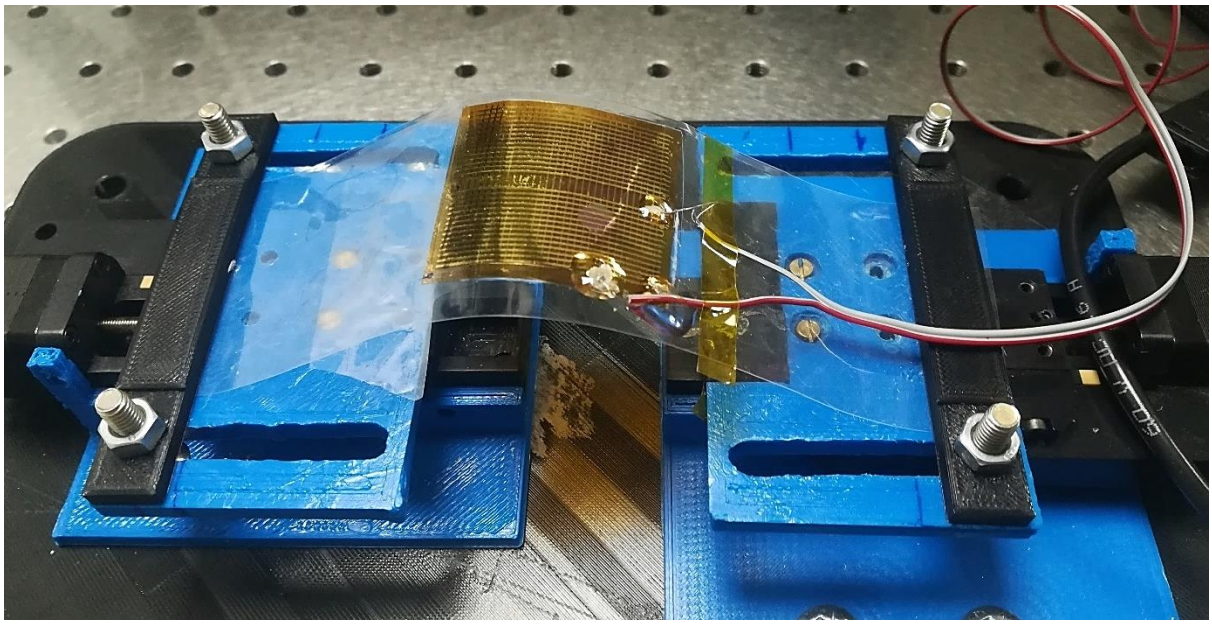

Annex I – Burned electrodes.

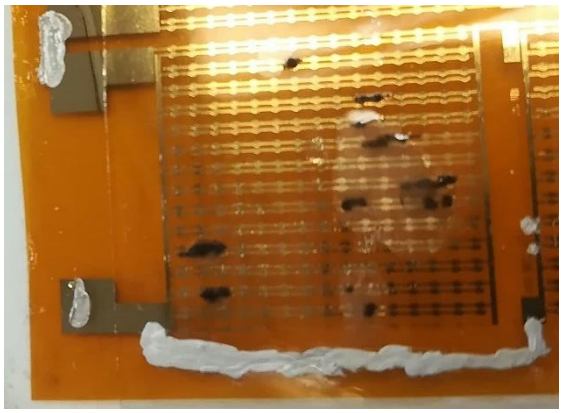

Annex J – Nanowire alignment and density analysed through SEM image with GT Fiber.

Annex L – Dielectrophoresis alignment with drop casting on top of the electrodes for thermal characterization.

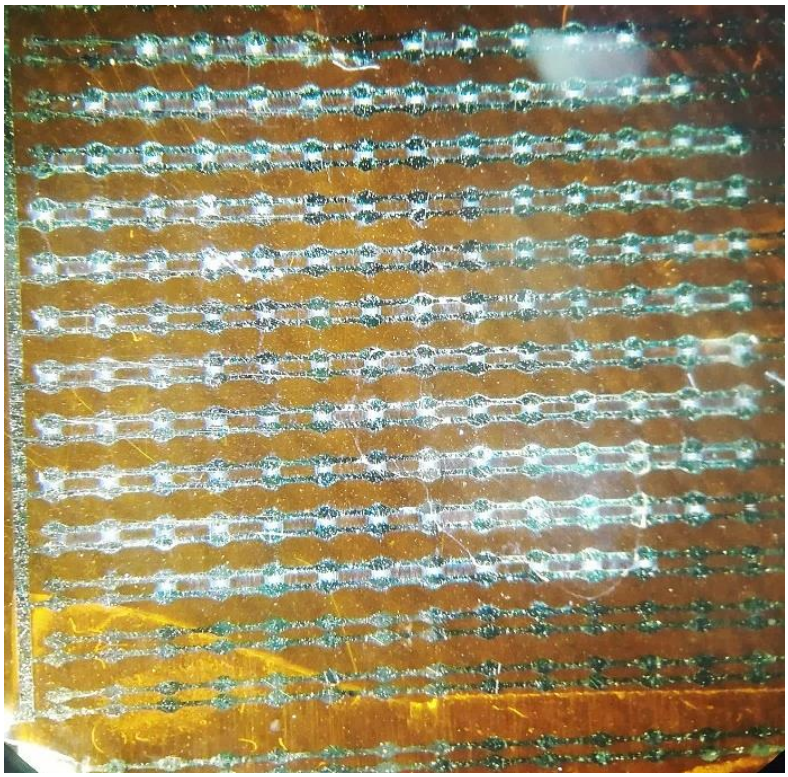

Annex M – TCR calculation with linear fitting.

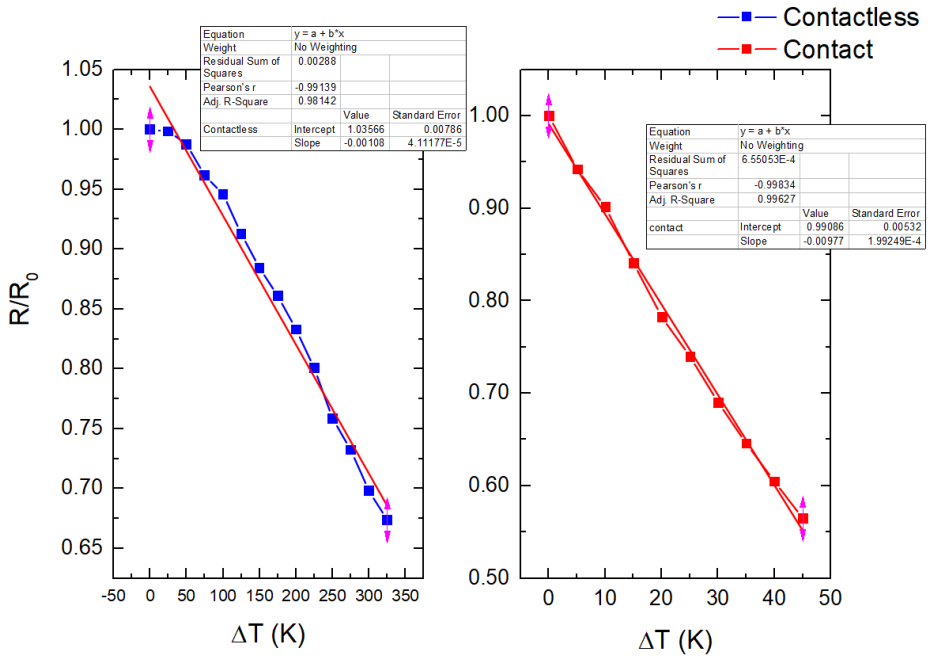

Annex N – Matlab code to calculate real part of F_{CM}.

```
FreqPow=0:0.1:15; %Frequency values from 0 to 15 with 0.1 step.

Epsilon0=8.857e-12; % F/m

EpsMed=80*Epsilon0;  %Dielectric constant of medium (H2O)
EpsilonParticle=25*Epsilon0;  %Dielectric constant of particle (V2O5)

ConductivityMedium=1e-6;  % Conductivity medium (H2O)
ConductivityParticle=50;  % Conductivity particle (V2O5)

RealClausMossatiFactor=zeros(length(FreqPow),1);
for(p=1:length(FreqPow))
    Freq=10^FreqPow(p);
       EpsilonMedium=EpsMed;

EpsilonPartComplex=EpsilonParticle-1i*ConductivityParticle/(6.28*Freq); %complex of the
particle

EpsilonMedComplex=EpsilonMedium-1i*ConductivityMedium/(6.28*Freq); %complex of the medium

FcmLong=(EpsilonPartComplex-EpsilonMedComplex)/(EpsilonMedComplex); %Fcm for lenght axis NW

Fcmshort=2*(EpsilonPartComplex-EpsilonMedComplex)/(EpsilonPartComplex+2*EpsilonMedComplex);
%Fcm for short axis NW

Fcmlongreal(p)=real(FcmLong);

Fcmshortreal(p)=real(Fcmshort);

end

plot(FreqPow, Fcmshortreal);

hold on

plot(FreqPow, Fcmlongreal);

hold off
```

Annex O – Comsol simulation gradient approximation.

Arrow volume coordinate equations

Ex - d((ec.Ex)^2+(ec.Ey)^2,x)

Ey - d((ec.Ex)^2+(ec.Ey)^2,y)

Ez - d((ec.Ex)^2+(ec.Ey)^2+(ec.Ez)^2,z)

Annex Q – EDS of new nanowire batch.

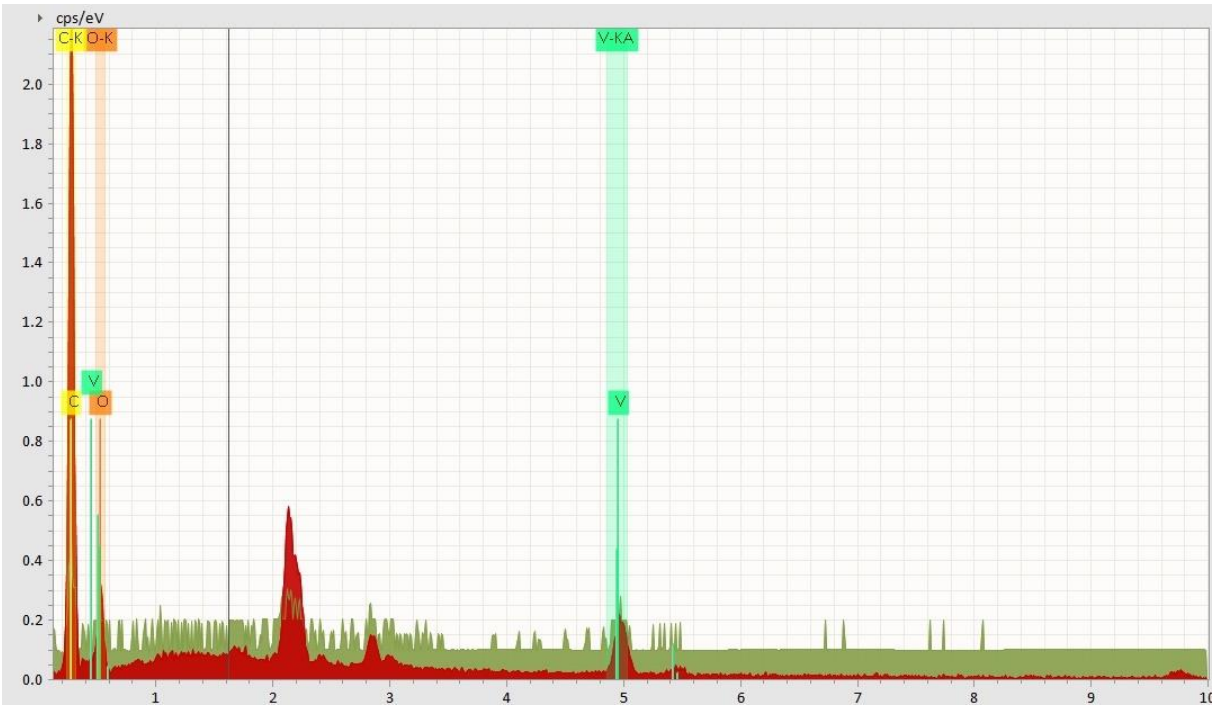

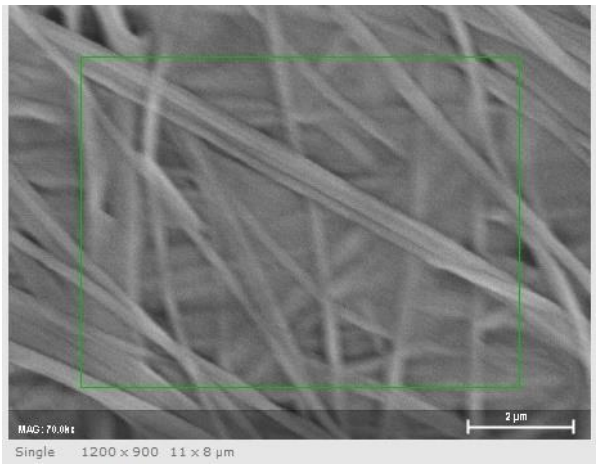

Reliability investigation of Via-bridges for flexible electronics

João Neto, Ayoub Zumeit, William Navaraj, Ravinder Dahiya*
Bendable Electronics and Sensing Technologies group, University of Glasgow, United Kingdom
*Ravinder.Dahiya@glasgow.ac.uk

I. Summary And Motivation

In this paper we have carried out investigation of reliability of Via-bridge under mechanical bending for application in flexible electronics. Progresses in the flexible electronics field unlocked the fabrication of next-generation devices such as foldable mobile phones, wearables [1], electronic skin (e-skin) [2-4], textile electronics [5], flexible energy harvesting/storage [2,5] and flexible memory devices [6,7].

As technology advances, a complex system level integration between several layers and types of components are required. A common strategy used for connecting these layers include the use of vertical interconnect access often known as Via. They enable the connection between layers allowing the design of a much more complex circuitry and 3D stacked applications. Example include electronic systems such as electronic skin [8][9], flexible displays [10], memory [6,7] etc. which typically involve passive or active matrix. However, one of the main concerns regarding the flexible/stretchable electronics is its mechanical reliability and robustness of both device and interconnections. The electrical properties of the system must not be affected during bending, guaranteeing that the performance is consistent through the system lifetime [11].

The Via-bridges presented in this paper were fabricated using standard microelectronic fabrication techniques. Row and column interconnects were fabricated to connect to array of electrodes. In the fabricated structure, column interconnects connect to the electrode through Via-bridges. The fabricated Via-bridges were tested under different degrees of mechanical bending. The bending test revealed a change in resistance during the bending strain and net resistance returns to normal values when the stress is removed. A maximum resistance variation of 12.9% was observed with bending curvature (R_C) of 1.85 cm. The Via-bridges were found to be stable for more than 1500 cycles of bending, thus showing the reliability of the Via-bridge.

II. Advances over Previous Works

Numerous Via fabrication techniques have been reported for flexible electronics namely mechanical [12], photolithography [13,14], inkjet printing [15,16], photoablation [17], laser drilling [18,19], solvent dissolution [20] and screen printing [21]. Conventional microelectronic fabrication techniques are widely used for realizing flexible electronics both for research as well as commercial applications. Here, we have carried out investigation of plugless Via-bridges comprising of Gold/Nichrome interconnects with PECVD SiO_x as insulator between them.

III. Results and Methodology

A. Schematic and Device Dimensions

Typically, a passive matrix array comprises of sensors and/or output passive elements addressed by row column interconnects. As a test structure to evaluate the reliability of the Via-bridges, we have fabricated an array of electrodes with the diagonal electrodes short circuited. The test structure comprises of 30 x 30 electrode pair arrays with row and column interconnects forming a passive matrix. The electrode pairs have 400 x 450 µm pad dimensions with a 30 µm gap between them. The full sample has 3.5 cm width and length, with the row and column insulated by PECVD SiO_x. The columns connect to the left pad of the electrode while the rows connect to the right pad of the electrode through Via-bridges as depicted in the figure 1. The rows and columns connect with each other only at the short-circuited diagonal electrodes so that every row is connected to one of the column electrodes. These pathways were probed for resistance change during bending analysis. The next section describes the fabrication of this test structure.

B. Device Fabrication

A sheet of polyimide (PI) of 50 µm thick was used as a substrate. The PI sheet was cleaned with acetone and IPA with ultrasonic agitation. Conventional UV lithography procedure was used for patterning the pads and the column electrodes with spin coated LOR10A/S1818 bilayer photoresist lift-off stack. A second UV exposure was carried out to short all the diagonal electrode pairs. Before metallization, a plasma surface treatment was done for 1 minute with 150 watts power, followed by metallization and lift-off. E-beam evaporation was used for

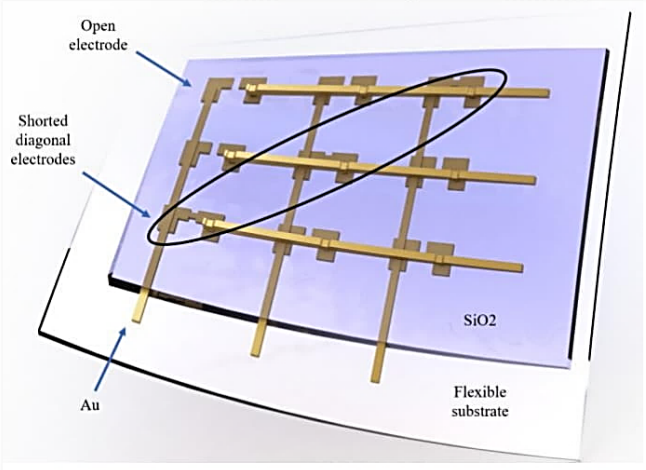

Fig. 1: Schematic of the fabricated interconnect structure with the bridged diagonal electrodes.

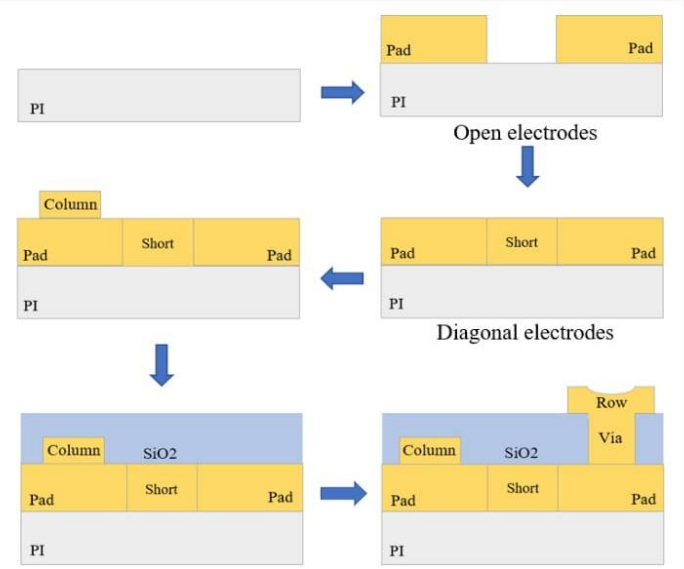

Fig. 2: Fabrication methodology steps.

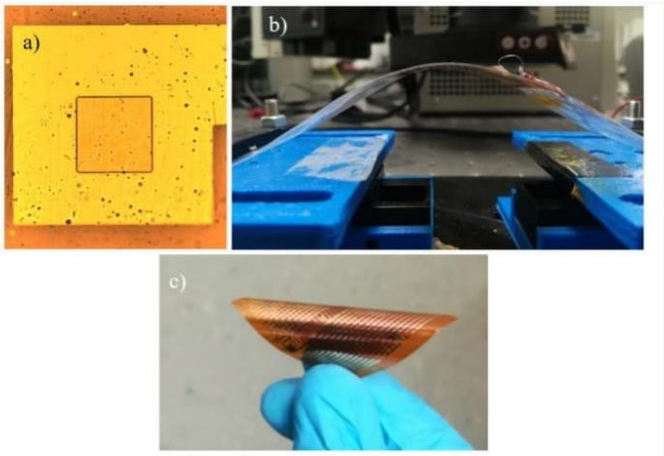

Fig. 3: a) Image of the via hole on the electrode pad. b) Bending setup; c) Final image of the fabricated sample.

metallization to deposit NiCr/Au/NiCr stack of thickness 10 nm/80 nm/10 nm respectively. This was followed by deposition of SiO_x of thickness 500 nm using PECVD and followed by another UV lithography process to open Via holes as shown in Fig. 3(a), with width of 170 µm on the right electrode pads. The SiO_x was etched using 5:1 buffered-oxide etchant (BOE) solution. Finally, the column interconnects were realized by another lithography and deposition of 10 nm/140 nm NiCr/Au stack was carried out using E-beam evaporation which bridges through the Via hole in the PECVD SiO_x to form contact with the right electrode pads.

C. Electrical characterization

Wires were bonded to the pads and one of the row-column diagonal pathways was electrically probed for the reliability analysis. The electro-mechanical characterization was carried out with a bending setup shown in Fig. 3(b) with Agilent 34461A 6.5-digit multimeter. The setup comprises of two jigs between which the sample was mounted, the bending was carried out by decreasing the gap between the jigs via a precision control motor. The electro-mechanical analysis was automated through a LabVIEW program.

The results of the analysis are shown in Fig. 5(a) and (b). The measured base resistance (R_0) of the probed Via-bridge pathway was ~92.2 Ω under flat condition. The net electrical resistance of the pathway (R_{Total}) comprise of several resistive components in series as shown in Fig. 4 namely, R_{Cl}, R_V and R_R, R_W corresponding to the column interconnect, via, the row interconnect, and the connecting wire resistances respectively.

R_{Cl}, R_V and R_R were theoretically estimated (Table 1) considering the dimension of corresponding interconnect in the array and defined by the parallel of the Au and NiCr stack. The wire resistances were measured with the multimeter (defined as R_{W1} and R_{W2}). R_{Total} is defined in equation 1 as the sum of all the resistances estimation which accounts for 17.9 Ω.

$$R_{Total} = R_{Cl} + R_R + R_V + R_{W1} + R_{W2} \quad (1)$$

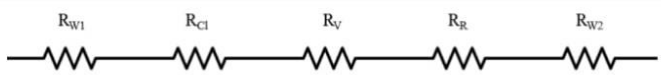

Fig. 4: Model of the series resistances.

TABLE I. VARIOUS RESISTIVE COMPONENTS

	R_{W1}/R_{W2}	R_{Cl}	R_R	R_V	R_{Total}
Ω	0.14/0.14	10.5	6.9	0.147	17.82

Fig. 5(a) shows the bending cycle with various radius of curvature (R_C). As observed, the relative change in the resistance increases with bending. Fig 5(b) shows the peak relative change in resistance Vs the R_C. The change in the resistance can be attributed to the piezoresistivity and influence of the stress on the Via contacts and interfaces. A maximum change to 117 Ω ($\Delta R/R_0 = 12.9\%$) was obtained for the lowest radius of curvature of 1.85 mm.

During and after the bending cycles the electrical properties of the device remained relatively unchanged for more than 1500 cycles proving the consistency of the Via-bridges.

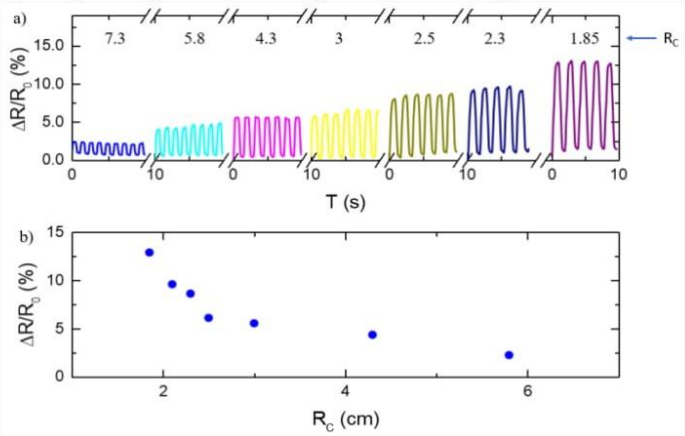

Fig. 5: a) Bending cycle test with varying R_C. b) Radius curvature Vs Peak Relative Change in Resistance (%).

ACKNOWLEDGEMENT

This work was supported in part by EPSRC Engineering Fellowship for Growth (EP/R029644/1 and EP/M002527/1).

REFERENCES

[1] C. G. Nunez, A. Vilouras, W. T. Navaraj, F. Liu, and R. Dahiya, ZnO Nanowires based Flexible UV Photodetector System for Wearable Dosimetry, IEEE Sensors Journal, Vol 18 (19), pp 7881-7888, 2018.

[2] C. G. Nunez, L. Manjakkal, and R. Dahiya, Energy Autonomous Electronic Skin, NPJ Flexible Electronics, Vol. 3, Art 1, 2019

[3] N. Yogeswaran, W. T. Navaraj, S. Gupta, F. Liu, V. Vinciguerra, L. Lorenzelli, and R. Dahiya, Piezoelectric Graphene Field Effect Transistor pressure Sensors for Tactile Sensing, Applied Physics Letters, Vol. 113, 014102, 2018.

[4] L. Manjakkal, B. Sakthivel, N. Gopalakrishnan, and R. Dahiya, Printed Flexible Electrochemical pH Sensors based on CuO Nanorods, Sensors and Actuators B: Chemical, Vol. 263, pp 50-58, 2018.

[5] L. Manjakkal, W. Dang, N. Yogeswaran, and R. Dahiya, Textile Based Potentiometric Electrochemical pH Sensor for Wearable Applications, Biosensors, Vol. 9(14), pp 1-12, 2019.

[6] Zhou, L., Mao, J., Ren, Y., Han, S. T., Roy, V. A. L., & Zhou, Y, Recent Advances of Flexible Data Storage Devices Based on Organic Nanoscaled Materials. Small, 14(10), 1–27, 2018.

[7] Ghoneim, M., Hussain, M., Ghoneim, M. T., & Hussain, M. M., Review on Physically Flexible Nonvolatile Memory for Internet of Everything Electronics. Electronics, 4(3), 424–479, 2015.

[8] K. Takei, T. Takahashi, J. C. Ho, H. Ko, A. G Gillies, P. W. Leu, R. S. Fearing, and A. Javey, Nanowire active-matrix circuitry for low-voltage macroscale artificial skin, Nature materials, vol. 9, no. 10, p. 821, 2010.

[9] W. T. Navaraj, C. García Núñez, D. Shakthivel, V. Vinciguerra, F. Labeau, D. Gregory, D. Dahiya, Nanowire FET based Neural Element for Robotic Tactile Sensing Skin, Frontiers in Neuroscience, vol. 11, pp. 1-20, 2017.

[10] T. Sekitani, H. Nakajima, H. Maeda, T. Fukushima, T. Aida, K. Hata, T. Someya, Stretchable active-matrix organic light-emitting diode display using printable elastic conductors, Nature Materials, volume 8, pages 494–499, 2009.

[11] Harris, K. D., Elias, A. L., & Chung, H.-J., Flexible electronics under strain: a review of mechanical characterization and durability enhancement strategies. Journal of Materials Science, 51(6), 2771–2805, 2016.

[12] Hart, C. M., De Leeuw, D. M., Matters, M., Herwig, P. T., Mutsaerts, C. M. J., & Drury, C. J., Low-cost all-polymer integrated circuits. *European Solid-State Circuits Conference*, *108*, 30–34, 1998.

[13] Gelinck, G. H., Geuns, T. C. T., & De Leeuw, D. M., High-performance all-polymer integrated circuits. *Applied Physics Letters*, *77*(10), 1487–1489, 2000.

[14] Nam, S., Jiang, X., Xiong, Q., Ham, D., & Lieber, C. M., Vertically integrated, three-dimensional nanowire complementary metal-oxide-semiconductor circuits. *Proceedings of the National Academy of Sciences*, *106*(50), 21035–21038, 2009.

[15] Sirringhaus, H., Kawase, T., Friend, R. H., Shimoda, T., Inbasekaran, M., Wu, W., & Woo, E. P., High-resolution inkjet printing of all-polymer transistor circuits. *Science (New York, N.Y.)*, *290*(5499), 2123–2126, 2000.

[16] Kawase, T. , Sirringhaus, H. , Friend, R. H. and Shimoda, T., Inkjet Printed Via ‐ Hole Interconnections and Resistors for All ‐ Polymer Transistor Circuits. Adv. Mater., 13: 1601-1605, 2001.

[17] Jain, K., Member, S., Klosner, M., & Zemel, M., Flexible Electronics and Displays : Lithography and Photoablation Processing Technologies for High-Throughput Production. *Technology*, *93*(8), 2001.

[18] Park, J., Lee, J., Park, S., Shin, K. H., & Lee, D., Development of hybrid process for double-side flexible printed circuit boards using roll-to-roll gravure printing, via-hole printing, and electroless plating. *International Journal of Advanced Manufacturing Technology*, *82*(9–12), 1921–1931, 2016.

[19] Kujala, M., Kololuoma, T., Keskinen, J., Lupo, D., Mantysalo, M., & Kraft, T. M., Screen Printed Vias for a Flexible Energy Harvesting and Storage Module. *International Flexible Electronics Technology Conference, IFETC 2018*.

[20] McKerricher, G., Perez, J. G., & Shamim, A., Fully inkjet printed RF inductors and capacitors using polymer dielectric and silver conductive ink with through vias. *IEEE Transactions on Electron Devices*, *62*(3), 1002–1009, 2015.

[21] Zhang, T., Asher, E., & Yang, J., A New Printed Electronics Approach Eliminating Redundant Fabrication Process of Vertical Interconnect Accesses: Building Multilayered Circuits in Porous Materials. *Advanced Materials Technologies*, *3*(4), 1–11, 2018.

Annex R – Table of constants used in the simulations.

Table 3 - Electrical constants used in simulations

Material	ε_r	σ *(S/m)*
Polyimide [37]	3.4	6.66×10^{-18}
Gold [38]	6.9	4.5×10^{6}
DI Water [23]	80	1×10^{-6}
PVC [37]	2.9	1×10^{-16}
Vanadium Pentoxide	25 *	50 [31]

* - The electrical properties of vanadium pentoxide by James McCulloch, 1968.

Annex S – Electric field gradient of PVC setup.